Title

Siddhartha Patra,[1,*] Abhirup Mukherjee,[1,†] Anirban Mukherjee,[1,2,‡] A. Taraphder,[3] and Siddhartha Lal[1,§]

[1] *Department of Physical Sciences, Indian Institute of Science Education and Research-Kolkata, W.B. 741246, India*
[2] *Ames Laboratory, Ames, Iowa 50011, USA*
[3] *Department of Physics, Indian Institute of Technology Kharagpur, Kharagpur 721302, India*

(Dated: January 24, 2022)

Lorem ipsum dolor sit amet, consectetuer adipiscing elit. Ut purus elit, vestibulum ut, placerat ac, adipiscing vitae, felis. Curabitur dictum gravida mauris. Nam arcu libero, nonummy eget, consectetuer id, vulputate a, magna. Donec vehicula augue eu neque. Pellentesque habitant morbi tristique senectus et netus et malesuada fames ac turpis egestas. Mauris ut leo. Cras viverra metus rhoncus sem. Nulla et lectus vestibulum urna fringilla ultrices. Phasellus eu tellus sit amet tortor gravida placerat. Integer sapien est, iaculis in, pretium quis, viverra ac, nunc. Praesent eget sem vel leo ultrices bibendum. Aenean faucibus. Morbi dolor nulla, malesuada eu, pulvinar at, mollis ac, nulla. Curabitur auctor semper nulla. Donec varius orci eget risus. Duis nibh mi, congue eu, accumsan eleifend, sagittis quis, diam. Duis eget orci sit amet orci dignissim rutrum.

Nam dui ligula, fringilla a, euismod sodales, sollicitudin vel, wisi. Morbi auctor lorem non justo. Nam lacus libero, pretium at, lobortis vitae, ultricies et, tellus. Donec aliquet, tortor sed accumsan bibendum, erat ligula aliquet magna, vitae ornare odio metus a mi. Morbi ac orci et nisl hendrerit mollis. Suspendisse ut massa. Cras nec ante. Pellentesque a nulla. Cum sociis natoque penatibus et magnis dis parturient montes, nascetur ridiculus mus. Aliquam tincidunt urna. Nulla ullamcorper vestibulum turpis. Pellentesque cursus luctus mauris.

CONTENTS

I. Introduction 1
A. Summary of Main Results: 2

II. Fixed point theory of over-screened MCK model 3
A. RG flows towards intermediate coupling 3
B. Star graph as the effective fixed point Hamiltonian 3

III. Important Properties of the Star Graph 4
A. Degree of compensation: a measure of the frustration 4
B. Impurity magnetization and susceptibility 5
C. Topological properties of ground state manifold 6
D. Local Mott liquid 7

IV. Local non-Fermi liquid excitations of the 2-channel Kondo 7
A. Effective Hamiltonian 7
B. Local Marginal Fermi liquid and Orthogonality catastrophe 9

V. Entanglement properties 10
A. Entanglement properties of the star graph 10
1. Impurity entanglement entropy 10
2. Mutual Information 11
3. Multipartite information 11
B. Entanglement properties of the multichannel Kondo fixed point 12
1. Impurity entanglement entropy 12
2. Intra-channel Mutual information 13
3. Bures distance and orthogonality catathrope 14

VI. Dualities of the multichannel Kondo model 15

VII. Impurity Quantum Phase transition in the multichannel Kondo model under channel anisotropy 15

VIII. Conclusions 16

Acknowledgments 17

References 17

I. INTRODUCTION

Understanding the nature of the low energy physics of multi-channel Kondo and the breakdown of screening remained a challenge. This work uses the recently developed unitary renormalization group (URG) technique to get the low energy effective Hamiltonian of this multi channel Kondo problem. We have already used this URG method to get the low energy effective Hamiltonian of the single-channel Kondo problem. This method has also been applied in many other strongly correlated problems [CITE]. We start with the multi-channel Kondo bare Hamiltonian; using this URG, we decouple electrons of higher energy from the rest to get the low energy effective Hamiltonian. Iteratively applying this URG method, we stop at a fixed point with a low energy fixed point Hamiltonian (LEH) with an intermediate Kondo coupling strength. We focus on the zero bandwidth limit where the problem reduces to a stargraph problem where one impurity spin S_d is talking to multiple spin 1/2s. We

have shown that most of the important properties of the multi-channel problem, like ground state degeneracy and breakdown of screening, can be understood by studying this stargraph problem. We find an exact duality between the over-screened and under-screened problems. In the exactly screened case, the impurity spin susceptibility at low temperature is independent of T saturating at a finite non-zero value against the power-law divergence $(1/T)$ for over and under-screened cases showing a clear distinction between them.

Apart from understanding this zero bandwidth model, we have also studied the role of excitations and derived the low energy effective Hamiltonian. We show the absence of local Fermi liquid in the overscreened multi-channel problem due to the degenerate groundstate manifold, in contrast to the exactly screened single-channel problem. The non-Fermi liquid structure of the LEH is purely coming out of a degenerate ground state manifold. We have studied different thermodynamic quantities of this effective Hamiltonian like specific heat, Susceptibility presented in the supplementary material. For the two-channel case, these measures obey logarithmic scaling with temperature as known in the literature. Along with various thermodynamics we have also studied different entanglement features of the ground state manifold of both the zero bandwidth star graph model and the multi-channel Kondo model. Though there is no direct inter-channel coupling in the Hamiltonian the strong inter-channel mutual information shows the presence of correlation among them in the degenerate ground state of the stargraph. Various entanglement measures show adiabatic continuity upon the addition of excitation for a single-channel case in contrast to the violation of it in the multi-channel case. This discontinuity shows a clear signature of orthogonality catastrophe in the multi-channel Kondo problem supporting the presence of local non-Fermi liquids independently. The ground state degeneracy of the zero-bandwidth multi-channel Kondo model is robust against anisotropy in the impurity-channel coupling strength. The degeneracy remains unchanged until some couplings vanish or diverge. Under URG we have verified that under channel anisotropy one gets to an effective multi-channel problem with a lower number of channels via a impurity quantum phase transition. The above two studies show that until the RG reaches the fixed point the degeneracy does not change. Below we present the summary of main results and the structure of the manuscript. The structure of the manuscript and the main results are presented below.

A. Summary of Main Results:

First in II A we show the intermediate coupling RG fixed point and its effective Hamiltonian using the URG formalism. Then in II B, we focus on the zero bandwidth limit of the multichannel Kondo problem, which is a stargraph problem. Here we describe various properties of this stargraph Hamiltonian, like the ground state degeneracy for exact, over, and under-screened cases. In III A we show the level of screening in all the three exact, over and under-screened cases via measuring the expectation of the stargraph Hamiltonian in the ground state called degree of compensation. This degree of compensation is maximum for the exactly screened case and decreases in the over and under-screened case. Later in III B our computation of low temperature impurity field susceptibility shows divergence following a power law $(1/T)$ for over, and under-screened cases against the saturation for exactly screened case shows the breakdown of screening in the former. Following impurity magnetization study also supports the above result. In III C we recreate the degenerate groundstate manifold using non-local twist and translation operators. Next in III D we decouple the impurity spin from all (K) baths and get the low energy effective all-to-all Hamiltonian, which is a local Mott liquid phase.

In the following part of the paper, we are interested in the physics of excitations added upon the zero bandwidth stargraph problem. Doing a degenerate perturbation theory in IV A we get low energy effective Hamiltonian (LEH) of the two-channel Kondo problem. Here we show the complete absence of local Ferm liquid due to the ground state degeneracy of the multichannel problem and the emergence of a local non-Fermi liquid phase. In IV B we show the presence of Marginal Ferm liquid signaling orthogonality catastrophe in the two-channel Kondo problem. Next in V we study various entanglement signatures of the low energy fixed-point ground state of the multichannel Kondo problem. First, in V A we study various entanglement properties like von-Neumann entanglement entropy of the impurity with the rest, mutual information, and multi-partite information scaling of the zero bandwidth (stargraph) model. Later, in V B we show the variation of various entanglement measures (impurity entanglement entropy, mutual information, Bures distance) as you increase the excitation via increasing the realspace hopping strength. In VI we show various dualities residing in the MCK problem. First, we present the strong-weak coupling duality of the MCK, and later, we discuss the over-under screened duality of the zero bandwidth model (stargraph). In VII we show the robustness of the stargraph ground state degeneracy against the impurity-channel coupling anisotropy, followed by the RG treatment of the channel anisotropy on the full MCK problem.

II. FIXED POINT THEORY OF OVER-SCREENED MCK MODEL

A. RG flows towards intermediate coupling

We start with the usual K-channel Kondo model Hamiltonian with isotropic couplings[1]:

$$H = \sum_{l} \left[\sum_{\substack{k \\ \alpha=\uparrow,\downarrow}} \epsilon_{k,l} \hat{n}_{k\alpha,l} + \frac{\mathcal{J}}{2} \sum_{\substack{kk' \\ \alpha,\beta=\uparrow,\downarrow}} \vec{S}_d \cdot \vec{\sigma}_{\alpha\alpha'} c^\dagger_{k\alpha,l} c_{k'\alpha',l} \right] . \tag{1}$$

Here, l sums over the K channels of the conduction bath, k, k' sum over all the momentum states of the bath and α, β sum over the two spin indices of a single electron. $\mathcal{J}$ is the Kondo spin-exchange coupling. $c_{k\alpha,l}$ is the fermionic field operator at momentum k, spin α and channel l. $\epsilon_{k,l}$ represents the dispersion of the l^{th} conduction channel. $\vec{\sigma}$ is the vector of Pauli matrices and $\vec{S}_d = \frac{1}{2}\vec{\sigma}_d$ is the impurity spin operator.

We have performed a renormalisation group analysis of the Hamiltonian using the recently developed URG method[2–8]. The RG proceeds by applying unitary transformations in order to block-diagonalize the Hamiltonian by removing number fluctuations of the high energy degrees of freedom. If the most energetic electronic state at the j^{th} RG step is $|j\rangle$ defined by the energy $D_{(j)}$, the Hamiltonian will in general not conserve the number of particles in this state: $\left[H_{(j)}, \hat{n}_j\right] \neq 0$. The unitary transformation $U_{(j)}$ will remove this number fluctuation at the next RG step:

$$H_{(j-1)} = U_{(j)} H_{(j)} U^\dagger_{(j)}, \quad \left[H_{(j-1)}, \hat{n}_j\right] = 0 \tag{2}$$

The unitary transformations are given in terms of a fermionic generator $\eta_{(j)}$:

$$U_{(j)} = \frac{1}{\sqrt{2}} \left(1 + \eta_{(j)} - \eta^\dagger_{(j)}\right), \quad \left\{\eta_{(j)}, \eta^\dagger_{(j)}\right\}_{\pm} = 1 \tag{3}$$

where $\{A, B\}_{\pm} = AB \pm BA$. The generator itself is given by the expression

$$\eta^\dagger_{(j)} = \frac{1}{\hat{\omega}_{(j)} - \text{Tr}\left(H_{(j)} \hat{n}_j\right)} c^\dagger_j \text{Tr}\left(H_{(j)} c_j\right) \tag{4}$$

The operator $\hat{\omega}_{(j)}$ encodes the quantum fluctuation scales arising from the interplay of the kinetic energy terms and the interaction terms of the Hamiltonian:

$$\hat{\omega}_{(j)} = H_{(j-1)} - H^i_{(j)} \tag{5}$$

$H^i_{(j)}$ is that part of $H_{(j)}$ that commutes with $\hat{n}_j$ but does not commute with at least one $\hat{n}_l$ for $l < j$. The RG continues up to energy D^* where a fixed point is reached from the vanishing of either the numerator or the denominator.

The derivation of the RG equation for the over-screened regime ($2S < K$) of the spin-S-impurity K-channel Kondo problem is shown in the supplementary materials. On decoupling circular isoenergetic shells at energies $D_{(j)}$, the change in the Kondo coupling at the j^{th} RG step, $\Delta\mathcal{J}_{(j)}$, is given by

$$\Delta\mathcal{J}_{(j)} = -\frac{\mathcal{J}^2_{(j)} \mathcal{N}_{(j)}}{\omega_{(j)} - \frac{D_{(j)}}{2} + \frac{\mathcal{J}_{(j)}}{4}} \left(1 - \frac{1}{2}\rho \mathcal{J}_{(j)} K\right) \tag{6}$$

$\mathcal{N}_{(j)}$ is the number of electronic states at the energy shell $D_{(j)}$. We work in the low quantum fluctuation regime $\omega_{(j)} < \frac{D_{(j)}}{2}$. There are three fixed points of the RG equation. One arises from the vanishing of the denominator, and was present in the single-channel Kondo RG equation as well[9]. As shown there, this fixed-point goes to $\mathcal{J}^* = \infty$ as the bare bandwidth of the conduction electrons is made large. The other trivial fixed point is the trivial one at $\mathcal{J}^* = 0$. The third fixed point is reached when the numerator vanishes: $\mathcal{J}^* = \frac{2}{K\rho}$[1,10–12]. Only the intermediate fixed point is found to be stable. This is consistent with results from Bethe ansatz calculations[13–18], CFT calculations[19–21], bosonization treatments[22,23] and NRG analysis[24,25].

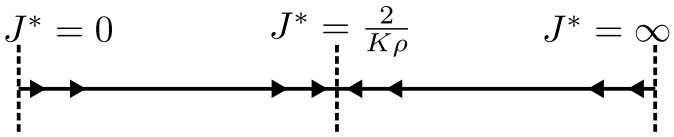

FIG. 1. The three fixed points of the over-screened RG equation. Only the intermediate one is stable.

The RG equation reduces to the perturbative form $\Delta\mathcal{J}_{(j)} \simeq \frac{\mathcal{J}^2_{(j)}\mathcal{N}_{(j)}}{D_{(j)}} \left(1 - \frac{1}{2}\rho\mathcal{J}_{(j)}K\right)$[1,11,12,26] when one replaces $\omega_{(j)}$ with the ground state energy $-\frac{D_{(j)}}{2}$ and assumes $\mathcal{J} \ll D_{(j)}$.

B. Star graph as the effective fixed point Hamiltonian

The fixed point Hamiltonian takes the form

$$H^* = \sum_{l} \left[\sum_{k}^{*} \epsilon_{k,l} \hat{n}_{k\alpha,l} + \mathcal{J} \sum_{kk'}^{*} \vec{S}_d \cdot \frac{1}{2} \vec{\sigma}_{\alpha\alpha'} c^\dagger_{k\alpha,l} c_{k'\alpha',l} \right] . \tag{7}$$

We have not explicitly written the decoupled degrees of freedom $D_{(j)} > D^*$ in the Hamiltonian. The $*$ over the summations indicate that only the momenta inside the window D^* enter the summation. There is an implied summation over the spin indices α, β.

To study the low energy physics and universality of the problem, we will mostly focus on the zero bandwidth limit of the fixed point Hamiltonian. Upon setting the chemical potential equal to the Fermi energy, this zero

bandwidth model becomes a Heisenberg spin-exchange Hamiltonian.

$$H^* = \mathcal{J}\sum_l \sum_{kk'}^{*} \vec{S}_d \cdot \frac{1}{2}\vec{\sigma}_{\alpha\alpha'} c^\dagger_{k\alpha,l} c_{k'\alpha',l} = \mathcal{J}\vec{S}_d \cdot \vec{S} \ . \quad (8)$$

At the last step, we defined the total bath local spin operator $S = \sum_l \vec{S}_l = \frac{1}{2}\sigma_l = \frac{1}{2}\sum_{kk'}^{*}\sum_{\alpha\beta}\vec{\sigma}_{\alpha\alpha'}c^\dagger_{k\alpha,l}c_{k'\alpha',l}$. The star graph commutes with several operators, including the total spin operator $J^z = S^z_d + S^z$ along z, the total bath local spin operator S^2 and the string operators

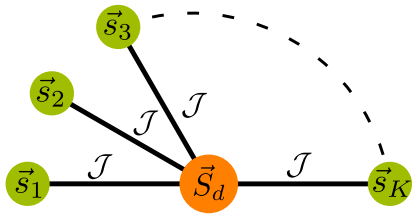

FIG. 2. [**COUPLING** $\mathcal{J}$] Zero bandwidth limit of the fixed point Hamiltonian. The central yellow node is the impurity spin, which is talking withe K green outer nodes that represent the local spins of the channels.

$$\pi^{x,y,z} = \sigma_d^{x,y,z} \otimes_{l=1}^{K} \sigma_l^{x,y,z} \ . \quad (9)$$

If we define the global spin operator $\vec{J} = \vec{S} + \vec{S}_d$, the star graph Hamiltonian can be written as $\mathcal{J}\left[J^2 - S_d^2 - S^2\right]$. The ground state is achieved for the maximal value of S, $S = \frac{K}{2}$, and the corresponding minimal value of J, $J = |\frac{K}{2} - S_d|$. This value corresponds to a multiplicity of $2J+1 = |K - 2S_d| + 1$ in J^z, and since the Hamiltonian does not depend on J^z, these orthogonal states $|J^z\rangle$ constitute a degeneracy of $g_K^{S_d} = |K - 2S_d| + 1$.

The π^z acts on the eigenstates $|J^z\rangle$ and reveals the odd-even parity of the eigenvalue J^z, and is hence a parity operator. Interestingly, the string operator π^z is a Wilson loop operator[27] that wraps around all the nodes of the star graph:

$$\pi^z = \exp\left[i\frac{\pi}{2}\left(\sigma_d^z + \sum_{l=1}^{K}\sigma_l^z - K\right)\right] = e^{i\pi\left(J^z - \frac{1}{2}K\right)} \quad (10)$$

π^x and π^y mix states of opposite parity. For example, it can be shown that $\pi^x |J^z\rangle = -|J^z\rangle$. These are 't Hooft operators[27].

There are multiple reasons for working with the star graph in particular and zero mode Hamiltonians in general. In the single-channel Kondo model, the star graph is just the two spin Heisenberg, and it reveals the stabilization of the Kondo model ground state, as well as certain thermodynamic properties (e.g., the impurity contribution to the susceptibility)[9,28–31]. Similarly in the MCK model, the star graph is able to mimic the nature of the RG flows: At weak coupling $\mathcal{J} \to 0^+$, the central spin is weakly coupled to the outer spins and prone to screening because of the $S^\pm$ terms in the star graph, and at strong coupling $\mathcal{J} \to \infty^-$, the outer spin-half objects tightly bind with the central spin-half object to form a single spin object that interacts with the remaining states through an exchange coupling which is RG relevant, rendering both the terminal fixed points unstable. The true stable fixed point must then lie somewhere in between, and we recover the schematic phase diagram of fig. 1.

The utility of the star graph is due to the fact that the non-Fermi liquid arises solely from the degeneracy of the ground state manifold of the underlying zero mode Hamiltonian, and the star graph captures this degeneracy in its entirety. The RG flows of the MCK model have been show to preserve the degeneracy of the ground state[24,32,33]. The star graph conserves the total spin J^z, and this leads to a ground state degeneracy of $|K - 2S_d| + 1$ in the $K-$channel spin-S_d impurity star graph which is preserved under the RG flow. This is qualitatively different from the case of the single-channel Kondo model where the $2-$fold degeneracy of the local moment fixed point crosses over into a stable and unique singlet ground state.

As we will see in a subsequent section, the lowest excitations of the intermediate fixed point is described a non-Fermi liquid phase induced by nearest-neighbour hopping terms between the zeroth sites and the first sites of the conduction channels. The importance of the degeneracy can be shown in the following manner. As mentioned previously, the ground state degeneracy of the more general star graph with a spin-S_d impurity and K channels is given by $g_K^{S_d} = |K - 2S_d| + 1$. The cases of $K = 2S_d$, $K < 2S_d$ and $K > 2S_d$ correspond to exactly screened, under-screened and over-screened regimes respectively. The latter two cases correspond to a multiply-degenerate manifold $g_K^S > 1$, and simultaneously have non-Fermi liquid phases[1,10,13,19,20,22,34–44], while the first regime has a unique ground state $g_K^S = 1$ and is described by a local Fermi liquid (LFL) phase[1,45–48], thereby substantiating the claim that a degeneracy greater than unity leads to non-Fermi liquid physics. In the following sections, we will show how the inherent quantum-mechanical frustration of singlet order that is present in the Hamiltonian leads to the degenerate ground state manifold and the non-trivial physics of the fixed points in terms of non-Fermi liquid phase, diverging thermodynamic quantities, quantum criticality as well as emergent gauge theories.

III. IMPORTANT PROPERTIES OF THE STAR GRAPH

A. Degree of compensation: a measure of the frustration

One can quantify the amount of screening of the local moment at the impurity site by defining a degree of compensation κ. Such a quantity also measures the inherent singlet frustration in the problem: the higher the degree of compensation, the better the spin can be

screened into a singlet and lower is the frustration. It is given by the antiferromagnetic correlation existing between the impurity spin and conduction electron channels: $\Gamma \equiv -\left\langle \vec{S}_d \cdot \vec{S} \right\rangle$. The expectation value is calculated in the ground state. Since the inner product is simply the ground state energy of a spin-S impurity $K-$channel MCK model in units of the exchange coupling J, we have

$$\Gamma = \frac{1}{2}\left[l_{\rm imp}^2 + l_c^2 - g_K^S\left(g_K^S - 1\right)\right] \tag{11}$$

$l_{\rm imp}^2 = S_d(S_d+1)$ is the length-squared of the impurity spin. Similarly, $l_c^2 = \frac{K}{2}\left(\frac{K}{2}+1\right)$ is the length-squared of the total conduction bath spin. $g_K^S = |K - S_d| + 1$ is the ground state degeneracy. We will explore the three regimes of screening by defining $K = K_0 + \delta, S = \frac{K_0}{2} - \delta$. $\delta = 0$ represents the exactly-screened case of $K = 2S = K_0$. Non-zero δ represents either over- or under-screening. In terms of K_0 and δ, the degree of compensation becomes

$$\Gamma = \frac{1}{4}\left[(K_0+1)^2 - (|\delta|+1)^2\right] \tag{12}$$

For a given K_0, the degree of compensation is maximised for exact screening $\delta = 0$, and is reduced for $\delta \neq 0$. This shows the inability of the system to form a unique singlet ground state and reveals the quantum-mechanical frustration inherent in the zero mode Hamiltonian and therefore in the entire problem. The degree of compensation is symmetric under the Hamiltonian transformation $\delta \to -\delta$, and this represents a duality transformation between over-screened and under-screened MCK models. This topic will be discussed in more detail later.

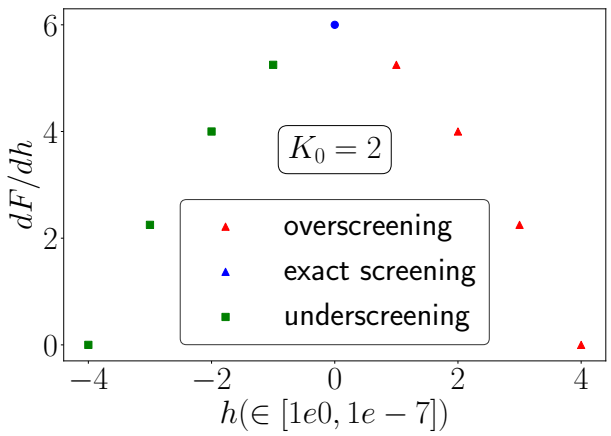

FIG. 3. Variation of the degree of compensation as we tune the system from under-screening to over-screening. The maximum spin compensation occurs at exact-screening $\delta = 0$.

B. Impurity magnetization and susceptibility

In order to obtain the magnetic susceptibility, We insert a magnetic field that acts only on the impurity and then diagonalize the Hamiltonian.

$$H(h) = \mathcal{J}^* \vec{S}_d \cdot \vec{S} + h S_d^z \tag{13}$$

The Hamiltonian commutes with S, so it is already block-diagonal in terms of the eigenvalues M of S. M takes values in the range $[M_{\rm min}, M_{\rm max}]$, where $M_{\rm max} = K/2$ for a $K-$channel Kondo model, and $M_{\rm min} = 0$ if K is even, otherwise $\frac{1}{2}$. Defining $\alpha = \frac{1}{2}(\mathcal{J}m + h) + \frac{\mathcal{J}}{4}$ and $x_m^M = M(M+1) - m(m+1)$, the partition function can be written as

$$Z(h) = \sum_{M=M_{\rm min}}^{M_{\rm max}} r_M^K \Bigg[\sum_{\substack{m=-M,\\ m\in\mathbb{Z}}}^{M-1} 2e^{\beta\frac{\mathcal{J}}{4}} \cosh\beta\sqrt{\mathcal{J}^2 x_m^M/4 + \alpha^2} + 2e^{-\beta\mathcal{J}M/2}\cosh\beta h/2 \Bigg] \tag{14}$$

Here, $\beta = \frac{1}{k_B T}$, M sums over the eigenvalues of S while m sums over $\mathcal{J}^z - \frac{1}{2}$ and the additional degeneracy factor $r_M^K = {}^{K-1}C_{K/2-M}$ arises from the possibility that there are multiple subspaces defined by $S = M$. To calculate the impurity magnetic susceptibility, we will use the expression

$$\chi = \frac{1}{\beta}\lim_{h\to 0}\left[\frac{Z''(h)}{Z(h)} - \left(\frac{Z'(h)}{Z(h)}\right)^2\right] \tag{15}$$

where the $'$ indicates derivative with respect to h. For brevity, we define $\theta_M = \beta\mathcal{J}(M+\frac{1}{2})/2$ and $\Sigma_M = \sum_{\substack{m=-M,\\ m\in\mathbb{Z}}}^{M-1}(m+\frac{1}{2})^2$. At low temperatures, the derivatives are

$$Z \to 2r_{M_{\rm max}}^K M_{\rm max} e^{\beta\frac{J}{2}(M_{\rm max}+1)} \tag{16}$$

$$Z'' \to r_{M_{\rm max}}^K \left(\frac{\beta}{2(M_{\rm max}+\frac{1}{2})}\right)^2 e^{\beta\frac{J}{2}(M_{\rm max}+1)}\Sigma_{M_{\rm max}} \tag{17}$$

$$\chi \to \frac{\beta\Sigma_{\rm max}}{2M_{\rm max}(2M_{\rm max}+1)^2} = \frac{\beta(K-1)}{12(K+1)} \sim \frac{1}{T} \tag{18}$$

The susceptibility is plotted in fig. 4.

This non-analyticity in a response function is a signature of the critical nature of the Hamiltonian. This is in contrast to the behaviour in the non-critical exactly-screened fixed point where the ground state is unique. There, the susceptibility becomes constant at low temperatures: $\chi(T\to 0) = \frac{W}{4T_K}$, T_K being the single-channel Kondo temperature and W the Wilson number[9,30,46,49]. We have checked the case of general spin-S impurity numerically (fig. 4), and the general conclusion is that all exactly-screened models show a constant impurity susceptibility at $T \to 0$, while the over-screened and under-screened cases show a diverging impurity susceptibility in the same limit.

A second non-analyticity arises when we consider the impurity free energy and the magnetization. The thermal free energy is given by

$$F(h) = -\frac{1}{\beta}\ln Z(h) = -\frac{1}{\beta}\ln\sum_{E_n} e^{-\beta E_n} \tag{19}$$

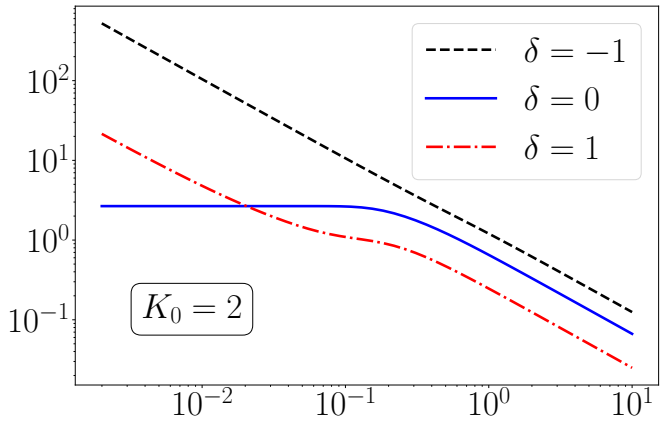

FIG. 4. Variation of impurity susceptibility against temperature. The exactly screened case ($\delta = 0$) saturates to a constant value at low temperatures, indicating complete screening. The cases of inexact screening show a divergence of the susceptibility, which means there is a remnant local spin at the impurity. Since the axes are in log scale, the behaviour is $\log T \sim -\log \chi$ which translates to $\chi \sim 1/T$.

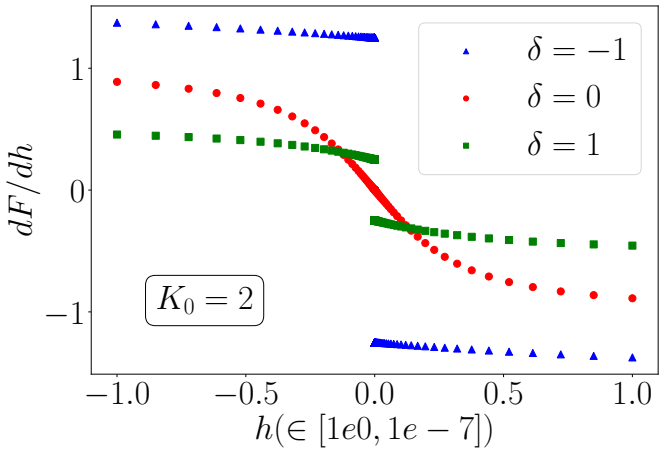

FIG. 5. Behaviour of the impurity magnetization for three values of $(K, 2S) = (2,4), (3,3), (4,2)$. Only the case of $K = 2S = 3\,(\delta = 0)$ is analytic near zero. The non-analyticity of the other cases arises because of the frustration brought about by the degeneracy of the star graph ground state.

At $T \to 0$, only the most negative energy $E_{\min}$ survives. The minimal energy eigenvalue is

$$E_{\min} = -\frac{J}{4} - \frac{1}{2}\sqrt{J^2(K+1)^2/4 + h^2 + |h|J(K-1)} \tag{20}$$

The first derivative of the free energy with respect to the field gives

$$F'(h \neq 0, T \to 0) = -\frac{2h + J(K-1)\text{sign}(h)}{4\sqrt{\frac{J^2}{4}(K+1)^2 + h^2 + |h|J(K-1)}} \tag{21}$$

There we used the result that the derivative of $|x|$ is $\text{sign}(x)$. If we now take h to zero from both directions, we get the magnetization of the impurity

$$m = F'(h \to 0^{\pm}, T \to 0) = \mp\frac{1}{2}\frac{(K-1)}{(K+1)} \tag{22}$$

The magnetization is therefore discontinuous as $h \to 0$; it goes to different values depending on the direction in which we take the limit. The non-analyticity for $K > 1$ occurs because there is at least one pair of ground state with non-zero parity π^z and magnetic field is able to flip one ground state into the state of opposite parity. This available space for scattering is simply the frustration that we discussed earlier. This argument, along with the diverging susceptibility for the over- and under-screened cases, makes it clear that the non-analyticity and hence the critical nature of the fixed point arise because of the ground state degeneracy, and is therefore a feature of all over-screened and under-screened models. Indeed, we have checked numerically (see fig. 5) that the non-analyticity exists for $\delta \neq 0$, where $\delta = \frac{K}{2} - S$ is the deviation from exact screening. For $\delta = 0$, the ground state is unique and unfrustrated, so the external magnetic field has no parity-inverted pair to flip across. Similar study can be done by putting an uniform field on all outer spins and calculating the susceptibility. Here also for all channles $K \geq 2$ the exponent is -1 supporting the existence of universality and criticality.

C. Topological properties of ground state manifold

We present the non-local twist and translation operators which can be used to explore the degenerate ground state manifold of the stargraph model. First we define two operators, for convenience let's call translation and twist operator respectively, $\hat{T}$ and $\hat{O}$ defined as

$$\hat{T} = e^{i\frac{2\pi}{K}\hat{\Sigma}}\ ,\ \hat{O} = e^{i\hat{\phi}}\ ,\quad \hat{\Sigma} = [\hat{J}^z - (K-1)/2] \tag{23}$$

One can see that the generators of these above operators commutes with the Hamiltonian, $[H, J^x] = [H, J^z] = [H, J^z] = 0$. In the large channel limit we can do semi-classical approximation. As J^x and J^y both commutes with the Hamiltonian H then $[H, J^y(J^x)^{-1}] = 0$, and any non-singular function of these operators must also commute with the Hamiltonian, thus we can say that

$$\hat{\phi} = \tan^{-1}(\hat{J}^y(\hat{J}^x)^{-1}) \tag{24}$$

Then we get $[\hat{\phi}, \hat{H}] = 0$. We can label the ground states by the eigenvalues of the translation operator $\hat{T}$. We can also use the ground states labeled by the eigenvalues of J^z (M, say). Then the ground states are

$$|M_1\rangle, |M_2\rangle, |M_2\rangle, \cdots, |M_K\rangle \tag{25}$$

Then the operations of the translation operators on this states are give below.

$$\hat{T}|M_i\rangle = e^{i\frac{2\pi}{K}[M_i - (K-1)/2]}|M_i\rangle = e^{i2\pi\frac{p_i}{K}}|M_i\rangle\ ,\ p_i \in [K] \tag{26}$$

Now we check the braiding rule between the twist and the translation operators, we find

$$\hat{T}\hat{O}\hat{T}^\dagger\hat{O}^\dagger = e^{\frac{2\pi}{K}[i\hat{\Sigma},i\hat{\phi}]} = e^{i\frac{2\pi}{K}}$$
$$\hat{T}\hat{O}^m\hat{T}^\dagger\hat{O}^{\dagger m} = e^{\frac{2\pi}{K}[i\hat{\Sigma},im\hat{\phi}]} = e^{i2\pi\frac{m}{K}} \quad (27)$$

Next, we shown that the states $\hat{O}^m|M_i\rangle$ are orthogonal to each other and with the state $|M_i\rangle$.

$$\hat{T}\hat{O}^m|M_i\rangle = \hat{O}^m\hat{T}e^{i2\pi\frac{m}{K}}|M_i\rangle = \hat{O}^m e^{i\frac{2\pi(m+p_i)}{K}}|M_i\rangle$$
$$\hat{T}\left(\hat{O}^m|M_i\rangle\right) = e^{i\frac{2\pi(m+p_i)}{K}}\left(\hat{O}^m|M_i\rangle\right) \quad (28)$$

Thus different states $\hat{O}^m|M_i\rangle$ for different m are labeled by different eigenvalues of the translation operations, thus are orthogonal to each other. Now as the twist operator $\hat{O}$ commutes with the Hamiltonian, thus we can see that

$$\langle M_i|\hat{O}^{m\dagger}H\hat{O}^m|M_i\rangle = \langle M_i|H|M_i\rangle \quad (29)$$

Thus the energy eigenvalues of all the orthogonal states are equal, which forms the K fold degenerate ground states. By the application of the twist operator $\hat{O}$ one can go from one degenerate ground states to another.

D. Local Mott liquid

Using the unitary renormalization group method we decouple the impurity spin from the zero-modes of the K channels. We start with the Hamiltonian. The zero mode Hamiltonian is a star graph model

$$H = \mathcal{J}\vec{S}_d.\sum_i \vec{S}_i = \mathcal{J}S_d^zS^z + \frac{\mathcal{J}}{2}(S_d^+S^- + S_d^-S^+)$$
$$H_D = \mathcal{J}S_d^zS^z \ , \quad H_X = \frac{\mathcal{J}}{2}(S_d^+S^- + S_d^-S^+) \quad (30)$$

Here we want to remove the quantum fluctuations between the impurity spin and the rest, for that we do one step URG.

$$\Delta H = H_X(\hat{\omega} - H_D)^{-1}H_X \quad (31)$$

In the zero mode IR fixed point ground state (star graph) of multichannel ground state J^z is a good quantum number but S^z is not. There is no net S^z field thus in the ground state manifold the average S^z is vanishing, $\langle S^z\rangle = 0$. We use this expectation value to replace the denominator of the above RG equation.

$$\beta_\uparrow(\mathcal{J},\omega_\uparrow) = (\mathcal{J}^2\Gamma_\uparrow)/2 \ , \quad \Gamma_\uparrow = (\omega_\uparrow - \mathcal{J}(S_d^z - 1))^{-1} \quad (32)$$

Thus we get the effective Hamiltonian is

$$H_{eff} = \frac{\beta_\uparrow(\mathcal{J},\omega_\uparrow)}{4}(S^+S^- + S^-S^+) \quad (33)$$

In terms of the electronics degree of freedom this looks

$$\frac{\beta_\uparrow(\mathcal{J},\omega_\uparrow)}{4}\sum_{\substack{i\neq j\\ \alpha_i,\beta_i\in\{\uparrow,\downarrow\}\\ \alpha_j,\beta_j\in\{\uparrow,\downarrow\}}} \vec{\sigma}_{\alpha_i\beta_i}\vec{\sigma}_{\alpha_j\beta_j}c_{0\alpha_i}^{(i)\dagger}c_{0\beta_i}^{(i)}c_{0\alpha_j}^{(j)\dagger}c_{0\beta_j}^{(j)} + \text{h.c.}$$

We will study the two cases of the above effective Hamiltonian depending on the sign of the prefactor. The case $\frac{\beta_\uparrow(\mathcal{J},\omega_\uparrow)}{2} > 0$ is the ferromagnetic case where in the ground state S takes the minimum value and S^z takes the possible maximum value. For an example, in the case of K channels the minimum value of S will be 0 or 1/2 for K being *even* or *odd* respectively. We will be interested in the other case where $\frac{\beta_\uparrow(\mathcal{J},\omega_\uparrow)}{2} < 0$. In this case the ground state corresponds to S being maximum and S^z being minimum case. The effective Hamiltonian can be re-written in this case as

$$H_{eff} = -|\beta_\uparrow(\mathcal{J},\omega_\uparrow)| \times (S^+S^- + S^-S^+)/4 \quad (34)$$

The CSCO of this Hamiltonian contains H, S, S^z. In the ground state S is maximum thus $S = K/2$ and S^z can take $2S+1 = K+1$ values. Thus in the largest S sector there are $K+1$ states. By the application of twist operator $\hat{Q} = \exp(i\hat{\phi}\Phi/\Phi_0)$, where $\hat{\phi}$ is the conjugate to $S6z$ folloing the algebra $[\phi,\hat{S^z}] = i$, we get the twisted Hamiltonian

$$H(\Phi) = -\frac{|\beta_\uparrow(\mathcal{J},\omega_\uparrow)|}{2}S^2 + \frac{|\beta_\uparrow(\mathcal{J},\omega_\uparrow)|}{2}\left(S^z - \frac{\Phi}{\Phi_0}\right)^2 \quad (35)$$

One can thus explore different S^z ground states via such flux tuning mechanism.

SHORTEN AND MERGE WITH THE EARLIER SUBSECTION For a K channel stargraph problem the ground state is K fold degenerate associated with different J^z values $\{-(K-1)/2, -(K-3)/2, \cdots, (K-1)/2\}$. After removing the quantum fluctuations between the impurity spin and the outer spins we get all-to-all model Eq.(35) as an effective Hamltonian. The eigen states of this all-to-all Hamiltonian can be labeled by S^z eigenvalues, there are $K+1$ such states made out of only the outer spins. The total state including the impurity spin can be written as $|J^z\rangle = |S_d^z\rangle\otimes|S^z\rangle$ labeled by $J^z = S_d^z + S^z$. As the all-to-all model has the Z_2 symmetry in impurity sector, there are $2(K+1)$ number of total states possible. For $S_d^z = 1/2$, $\{J^z\} = \{-(K-1)/2, \cdots, (K-1)/2, (K+1)/2\}$ and for $S_d^z = -1/2$, $\{J^z\} = \{-(K+1)/2, -(K-1)/2, \cdots, (K-1)/2\}$. We can see that in both the cases all K states of the stargraph ground state manifold is present in all-to-all model, this time any one those is ground state. Using the twist operator we can go from one ground state to other.

IV. LOCAL NON-FERMI LIQUID EXCITATIONS OF THE 2-CHANNEL KONDO

A. Effective Hamiltonian

RADICALLY SHORTEN! Here we start with the stargraph model Hamiltonian for the two-channel Kondo obtained under URG treatment. Our goal here is to add excitations on top of this stargraph state and get the low

energy effective Hamiltonian using degenerate perturbation theory.

$$H^{(2)} = \mathcal{J}\vec{S}_{imp}.(\vec{S}_1 + \vec{S}_2) \ \ , \ \ \vec{S}_i = \frac{1}{2}\, c^{\dagger}_{i,\alpha}\, \vec{\sigma}_{\alpha,\beta}\, c_{i,\beta} \quad (36)$$

Here $\vec{S}_i = 1, 2$ represents the spin degree of freedom present in the origin of the i^{th} channel. This two channel Hamiltonian has $2^3 = 8$ states in the eigenspectrum **CITESLAL**. There are two degnerate ground states labeled by $|J^z = +1/2\rangle, |J^z = -1/2\rangle$ with energy $-\mathcal{J}$ and 6 excited states. On top of the zero mode spin-channel interactions we want to consider the effect of the momentum space kinetic energy term $\sum_k \epsilon_k(n_{1,k} + n_{2,k})$ assuming identical dispersion for both the channels. Our zero mode spin Hamiltonian is written in the real space, thus it will be easier to do the perturbation theory in the real space. The Fourier transformation of the momentum space kinetic energy term leads to real space hopping term. For simplicity we will be considering only nearest neighbor hopping between sites within each channels. The real space hopping contribution to the Hamiltonian H_X with the hooping strength is

$$H_X = -t \sum_{\substack{<1,l_1> \\ <2,l_2>}} (c^{\dagger}_{1,\sigma} c_{l_1,\sigma} + c^{\dagger}_{2,\sigma} c_{l_2,\sigma} + \text{ h.c.}) \quad (37)$$

Here l_i represents the nearest site to the origin of the i^{th} channel. The perturbation H_X contains scattering which takes the states of the zero mode Hamiltonian out of spin-channel scattering space. For simplicity we will be keeping only one neareast neighbor to the origin of each channel. Thus before we start the perturbation theory we must expand the basis of the zero mode Hamiltonian itself. The basis we are intersted in is $\{\mathcal{B}_{extnd}\}$ given as

$$\{|S^z_{imp}, n_{1,\uparrow}, n_{1,\downarrow}, n_{2,\uparrow}, n_{2,\downarrow}\rangle \otimes |n_{l_1,\uparrow}, n_{l_1,\downarrow}, n_{l_2,\uparrow}, n_{l_2,\downarrow}\rangle\}$$

Note there are $2^4 = 16$ elements in the subspace $\{|n_{l_1,\uparrow}, n_{l_1,\downarrow}, n_{l_2,\uparrow}, n_{l_2,\downarrow}\rangle\}$. In the spin-channel basis $\{\mathcal{B}\}$ there 2 degenerate ground states. Because the unperturbed Hamiltonian $\mathcal{H}_0$ has no scattering terms outside the spin sector, in the extended basis $\{\mathcal{B}_{extnd}\}$ the total ground state degeneracy becomes simply 2×2^4, 32 fold. Thus the total Hamiltonian we are interested in is

$$\mathcal{H} = \frac{\mathcal{J}\hbar}{2}\ \vec{S}_d. \sum_{i=\{1,2\}} \sum_{\alpha,\beta\in\{\uparrow,\downarrow\}} c^{\dagger}_{i\alpha} \vec{\sigma}_{\alpha\beta} c_{i\alpha} + H_X \quad (38)$$

Thus, in the expanded basis there are 32 degnerate states given as

$$|\tilde{\alpha}_0\rangle = |J^z = +1/2\rangle \otimes |n_{l_1,\uparrow}, n_{l_1,\downarrow}, n_{l_2,\uparrow}, n_{l_2,\downarrow}\rangle \quad (39)$$
$$|\tilde{\alpha}_1\rangle = |J^z = -1/2\rangle \otimes |n_{l_1,\uparrow}, n_{l_1,\downarrow}, n_{l_2,\uparrow}, n_{l_2,\downarrow}\rangle \quad (40)$$

Using degenerate perturbation theory we calculate the first and the second order corrections to the Hamiltonian. The first order and the second order low energy effective Hamiltonian is given as

$$H^{(1)} = \sum_{ij} |\alpha_i\rangle\langle\alpha_i|V|\alpha_j\rangle\langle\alpha_j|$$
$$H^{(2)} = \sum_{ij}\sum_{l} |\alpha_i\rangle \frac{\langle\alpha_i|V|\mu_l\rangle\langle\mu_l|V|\alpha_j\rangle}{E_0 - E_l}\langle\alpha_j| \quad (41)$$

where $|\alpha_i\rangle$ represents the ground states with energy E_0 and μ_l represents the excited states with energy E_l. One can easily check the diagonal term in effective Hamiltonian coming from the 1^{st} or any *odd* order correction is zero as the state never returns to the original starting state. For the case of first order the off-diagonal correction to the effective Hamiltonian is also zero. In the second order we get both diagonal and off-diagonal contribitions to the effective Hamiltonian. Total diagonal contribution is coming from the two states $|\tilde{\alpha}_0\rangle$ and $|\tilde{\alpha}_1\rangle$, individually fiven as $H^{(2)}_{diag}(1/2)$,$H^{(2)}_{diag}(-1/2)$ respectively.

$$H^{(2)}_{diag}(1/2) = \frac{2t^2}{E_0}\hat{I} - \Omega_l \ , \ H^{(2)}_{diag}(-1/2) = \frac{2t^2}{E_0}\hat{I} + \Omega_l \quad (42)$$

where $S^z_{l_i} = (n_{l_i\uparrow} - n_{l_i\downarrow})/2$ and $\Omega_l = \frac{2t^2}{3E_0}(S^z_{l_1} + S^z_{l_2})$. Thus the total contribution to the diagonal effective Hamiltonian is $H^{(2)}_{diag} = -4t^2\hat{I}$, shows the absence of local Fermi liquid due to the exact cancellation of the field term. The off-diagonal contributio to the second order effective Hamiltonian is

$$\begin{aligned} H_{NFL} = H^{(2)}_{off} &= \sum_{i\neq j}\sum_{l} |\alpha_i\rangle \frac{\langle\alpha_i|V|\mu_l\rangle\langle\mu_l|V|\alpha_j\rangle}{E_0 - E_l}\langle\alpha_j| \\ &= -\frac{8t^2}{3}[(S^z_1)^2 c^{\dagger}_{2\uparrow} c_{2\downarrow}(c_{l_1\uparrow} c^{\dagger}_{l_1\downarrow} + c_{l_2\uparrow} c^{\dagger}_{l_2\downarrow}) \\ &+ (S^z_2)^2 c^{\dagger}_{1\uparrow} c_{1\downarrow}(c_{l_1\uparrow} c^{\dagger}_{l_1\downarrow} + c_{l_2\uparrow} c^{\dagger}_{l_2\downarrow})] + \text{h.c.} \ , \end{aligned} \quad (43)$$

This LEH is purely a non-Fermi liquid. The emergence of non-Fermi liquid is primarily coming due to the degenerate ground state manifold. Using this low energy effective Hamiltonian we have calculated different thermodynamic quatitites like susceptibility and specific heat. Both these measures shows logarithmic behavior at low temperature which is in agreement with known result in literature. These results are shown in the Supplementary material. In a similar way, we have calculated the LEH for the three channel Kondo. We find the absence of Fermi liquid in 2^{nd} order and the presence of non-Fermi liquid in the off-diagonal low energy effective Hamiltonian shown in the supplementary material.

MENTION THAT WE HAVE COMPUTED VARIOUS THERMODYNAMIC QUANTITIES THAT ARE IN FAIR AGREEMENT WITH THE LITERATURE. AND THAT THESE ARE SHOWN IN THE SUPPLEMENTARY MATERIALS. ALSO MENTION THAT WE HAVE ALSO DERIVED AN EFFECTIVE HAMILTONIAN FOR THE THREE CHANNEL CASE, ALSO SHOWN IN SUPPLEMENTARY MATERIALS.

B. Local Marginal Fermi liquid and Orthogonality catastrophe

The real space local low energy Hamiltonian that takes into account the excitations above the ground state is given by eq. 43 and can be written as

$$V_{\text{eff}} = \frac{2t^2}{\mathcal{J}^*}\left[\left(\sigma^z_{0,1}\right)^2 s^+_{0,2} + \left(\sigma^z_{0,2}\right)^2 s^+_{0,1}\right]\left(s^-_{1,1} + s^-_{1,2}\right) + \text{h.c.} \tag{44}$$

where $\sigma^z_{0,l} = \hat{n}_{0\uparrow,l} - \hat{n}_{0\downarrow,l}$, $s^+ = c^\dagger_{0\uparrow,l} c_{0\downarrow,l}$ and $s^- = (s^+)^\dagger$. The notation $0\sigma, l$ has the site index $i = 0, 1, 2, \ldots$ as the first label, the spin index $\sigma = \uparrow, \downarrow$ as the second label and the channel index $l = 1, 2$ as the third index.

These are the terms that are generated because of the presence of the impurity. Such a non-Fermi liquid (NFL) contribution to the effective Hamiltonian and the absence of any Fermi-liquid term at the same order should be contrasted with the local Fermi liquid excitations induced by the singlet ground state of the single-channel Kondo model[30,46,50].

We now take the MCK Hamiltonian to strong-coupling, and perform a perturbative treatment of the hopping. At $J \to \infty$, the perturbative coupling t^2/J is arbitrarily small and we again obtain Eq. 44. Such a change from the strong coupling model with parameter J to a weak coupling model with parameter t^2/J amounts to a duality transformation[32,33]. It can be shown that the duality transformation leads to an identical MCK model[32] (self-duality), which implies we can have identical RG flows, and our transformation simply extracts the NFL piece from the dual model. The self-duality also ensures that the critical intermediate-coupling fixed point is unique and can be reached from either of the models.

The diagonal part of eq. 44 is

$$V_{\text{eff}} = \frac{2t^2}{J}\sum_{l=1,2}\left(\sum_\sigma \hat{n}_{0\sigma,l}\right) s^+_{0,\bar{l}} s^-_{1,\bar{l}} + \text{h.c.} \tag{45}$$

where $\bar{l} = 3 - l$ is the channel index complementary to l. We will Fourier transform this effective Hamiltonian into $k-$space. The NFL part becomes

$$\sum_{\sigma,\{k_i,k'_i\},l} \frac{2t^2}{J} e^{i\left(k_1 - k'_1\right)a} c^\dagger_{k\sigma,l} c_{k'\sigma,l} c^\dagger_{k_2\uparrow,\bar{l}} c_{k'_2\downarrow,\bar{l}} c^\dagger_{k_1\downarrow,\bar{l}} c_{k'_1\uparrow,\bar{l}} + \text{h.c.} \tag{46}$$

This form of the Hamiltonian is very similar to the three-particle interaction term in Appendix B of[2]. The channel indices in Eq. 46 can be mapped to the normal directions in[2]. The 2 particle-1 hole interaction in Eq. 46 has a diagonal component which can be obtained by setting $k = k', k_1 = k'_2$ and $k_2 = k'_1$:

$$\begin{aligned} H_{\text{eff,MFL}} &= \sum_{\substack{k,k_1,\\ k_2,\sigma,l}} \frac{2t^2 e^{i(k_1-k_2)a}}{J} \hat{n}_{k\sigma,l}\hat{n}_{k_2\uparrow,\bar{l}}\left(1 - \hat{n}_{k_1\downarrow,\bar{l}}\right) + \text{h.c.} \\ &= \sum_{\substack{k,k_1,\\ k_2,\sigma,l}} \frac{4t^2}{J}\cos a\left(k_1 - k_2\right)\hat{n}_{k\sigma,l}\hat{n}_{k_2\uparrow,\bar{l}}\left(1 - \hat{n}_{k_1\downarrow,\bar{l}}\right) \end{aligned} \tag{47}$$

The most dominant contribution comes from $k_1 = k_2 = k'$, revealing the non-Fermi liquid metal[16,39]:

$$H^*_{\text{eff,MFL}} = \frac{4t^2}{J}\sum_{\sigma,k,k',l} \hat{n}_{k\sigma,l}\hat{n}_{k'\uparrow,\bar{l}}\left(1 - \hat{n}_{k'\downarrow,\bar{l}}\right) \tag{48}$$

A non-local version of this effective Hamiltonian was found to describe the normal phase of the Mott insulator of the 2D Hubbard model, as seen from a URG analysis[2,3]. Following[2], one can track the RG evolution of the dual coupling $R_j = \frac{4t^2}{J_j}$ at the j^{rh} RG step, in the form of the URG equation

$$\Delta R_j = -\frac{R_j^2}{\omega - \epsilon_j/2 - R_j/8} \tag{49}$$

In the RG equation, ϵ_j represents the energy of the j^{th} isoenergetic shell. It is seen from the RG equation that R is relevant in the range of $\omega < \frac{1}{2}\epsilon_j$ that has been used throughout, leading to a fixed-point at $R^*/8 = \omega - \frac{1}{2}\epsilon^*$). The relevance of R is expected because the strong coupling J is irrelevant and $R \sim 1/J$.

The renormalisation in R leads to a renormalisation in the single-particle self-energy[2]. The $k-$space-averaged self-energy renormalisation is

$$\Delta\Sigma(\omega) = \rho R^{*2}\int_0^{\epsilon^*} \frac{d\epsilon_j}{\omega - \epsilon_j/2 + R_j/8} \tag{50}$$

The density of states can be approximated to be N^*/R^*, where N^* is the total number of states over the interval R^*. As suggested by the fixed point value of R_j, we can approximate its behaviour near the fixed point by a linear dependence of the dispersion ϵ_j. The two limits of the integration are the start and end points of the RG. We start the RG very close to the Fermi surface and move towards the fixed point ϵ^*. Near the start point, we substitute $\epsilon = 0$ and $R = \omega$, following the fixed point condition. From the fixed point condition, we also substitute $R^*/8 = \omega - \frac{1}{2}\epsilon^*$. On defining $\bar{\omega} = N^*\left(\omega - \frac{1}{2}\epsilon^*\right)$, we can write

$$\Delta\Sigma(\omega) \sim \bar{\omega}\ln\frac{N^*\omega}{\bar{\omega}} \tag{51}$$

The self-energy also provides the quasiparticle residue for each channel[2]:

$$Z(\bar{\omega}) = \left(2 - \ln\frac{2\bar{\omega}}{N^*\omega}\right)^{-1} \tag{52}$$

As the energy scale $\omega \to 0$, the Z vanishes, implying that the ground state and lowest-lying excitations, in the presence of the NFL terms, are not adiabatically connected to the Fermi gas. This is the orthogonality catastrophe[51–54] in the two-channel Kondo problem, and it is brought about by the presence of the terms in Eq. 48. Such terms were absent in the single-channel Kondo model, because there was no multiply-degenerate ground state manifold that allowed scattering. This line of argument shows that the extra degeneracy of the ground state subspace and the frustration of the singlet order that comes about when one upgrades from the single-channel Kondo model to the MCK models is at the heart of the NFL behaviour, and the orthogonality catastrophe should be a general feature of all such frustrated MCK models. A local NFL term was also obtained by Coleman, et al.[40] in terms of Majorana fermions at the zeroth site and the first site of the $\sigma - \tau$ version of the two-channel Kondo model. There, they computed a self-energy of the form in eq. 51. The common features show the universality between the two-channel Kondo and the $\sigma - \tau$ models. ,

V. ENTANGLEMENT PROPERTIES

MINIMISE THE WORDS RADICALLY!

A. Entanglement properties of the star graph

For a K channel stargraph model we compute various entanglement measures in each of the K degenerate ground states labeled by the J^z eigenvalues as $|J^z\rangle$.

1. *Impurity entanglement entropy*

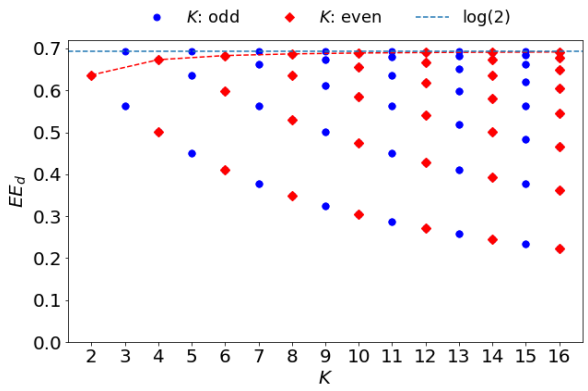

FIG. 6. Variation of impurity entanglement entropy (EE_d) with the rest for different channels (K). The maximum entropy in the large K limit is $\log 2$.

Here we are interested in finding the entanglement of the central impurity spin with the rest. For single channel case the ground state is unique which is $|J=0, J_z=0\rangle = \frac{1}{\sqrt{2}}(|\uparrow_d\downarrow_0\rangle - |\downarrow_d\uparrow_0\rangle)$. Thus the impurity entanglement enotropy is maximum $\log 2$. In the K cahnnel case we compute the impurity entanglement entropy (EE_d) in all the K degenerate ground states. The EE_d in the states $|\pm J^z\rangle$ is same. The state $|J^z\rangle \equiv |S_d = 1/2, S = K/2; (S-1/2), J^z\rangle$ has the density matrix $\rho = |J^z\rangle\langle J^z|$ from which we can calculate the reduced density matrix by partial tracing the impurity degree of freedom

$$\rho_d = \mathrm{Tr}_d \rho = \sum_{S_d^z} \langle S_d^z|\rho|S_d^z\rangle \ , \quad EE_d = -\rho_d \log \rho_d \quad (53)$$

The eigenvalues of this reduced density matrix given by λ_i is called entanglement spectrum. We compute such impurity entanglement entropy for various channels as shown in the Fig.6. The minimum entanglement entropy (associated with the $|J^z = J\rangle$ state) decreases with the increase of channel number. On the other hand the maximum entanglement entropy (associated with $|J^z_{min}\rangle$ state) is saturating at $\log 2$. Similar study has been done

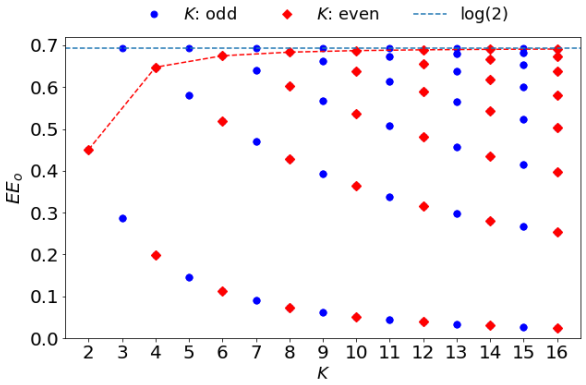

FIG. 7. Variation of the entanglement entropy of an outer spin (EE_o) with the rest for different channels (K). The maximum entanglement entropy in the large K limit is $\log 2$.

to calculate entanglent entropy of outer spin with the rest called EE_o shown in the Fig.7. We find a similar result where, the minimum entanglement entropy is associated with the state $|J^z = J\rangle$ and approaching zero in the limit $K \gg 1$. On the otherhand maximum entanglement entropy associated with the state $|J^z_{min}\rangle$ is saturating at a value $\log 2$ in the limit $K \gg 1$. Above entanglement study shows that, in the $|J^z_{min}\rangle$ state impurity and any outer spin is maximally entangled with the rest for the odd channel or in general for the large channel case. Both the impurity and outer-spin entanglement entropy with the rest is same in both the states $|\pm J^z\rangle$, which shows that interms of these entanglement entropy there is a parity symmetry between the states $|J^z\rangle$ and $\pi^x|J^z\rangle$. In the odd channel cases there is a unique $|J^z = 0\rangle$ state with a maxium entanglement entropy.

2. Mutual Information

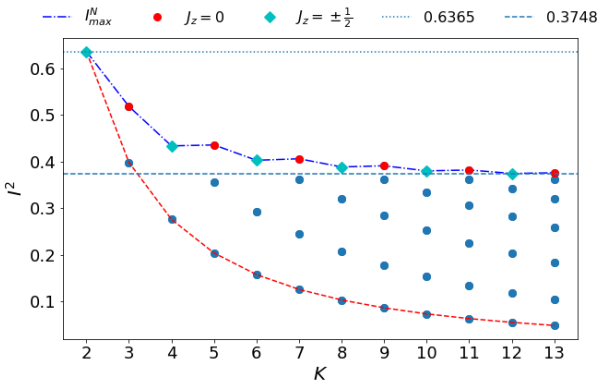

FIG. 8. Variation of mutual information ($I^2(d:o)$) with the rest for different channels (K). The maximum mutual informaiton is saturating at 0.37.

Mutual information is a measure which captures the correlations present between two subsystems (A,B) in a particular state defined as

$$I^2(A:B) = S_A + S_B - S_{A\cup B} \tag{54}$$

where S_A is the von-Neumann entanglement entropy of the subsystem A with the rest. Here we are interested in computing two types of mutual information first, study the mutual information between the impurity-spin (Fig.8) and second any one outer spin $I^2(d:o)$ and mutual information between two outer spins $I^2(o:o)$ (Fig.9) for various channels. In both cases we find that maximum and minimum mutual information is associated with the $|J^z_{min}\rangle$ and $|J^z = J\rangle$ state. We also find that mutual information in the states $|J^z\rangle$ and $\pi^x|J^z\rangle$ are same showing the parity symmetry in the mutual information measure. In the large channel limit ($K \gg 1$) the maximum mutual information is saturating to a same value (0.375) for

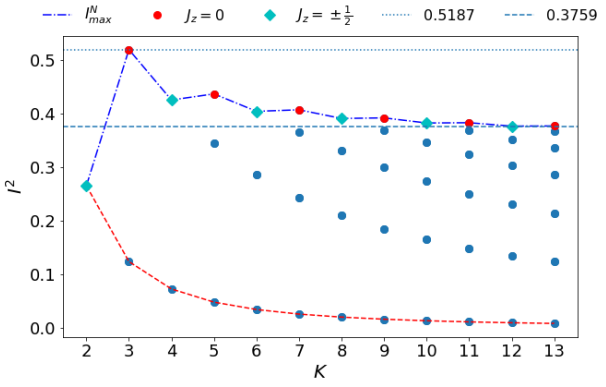

FIG. 9. Variation of mutual information ($I^2(o:o)$) with the rest for different channels (K). The minimum mutual inforamtion is vanishing in the large K limit.

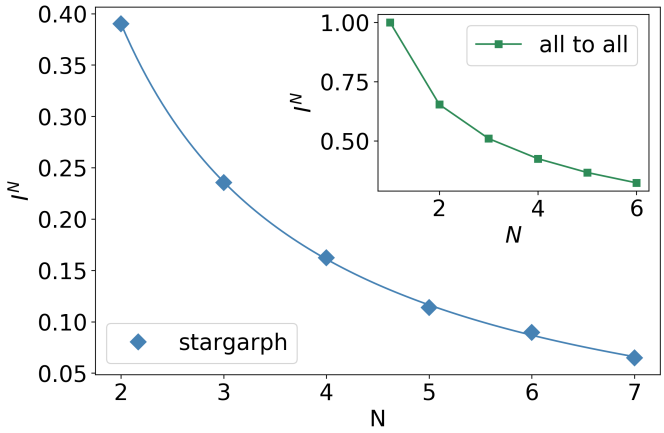

FIG. 10. Variation of multi-partite information I^N among the outer spins as a function of N for the multi channel case with $K = 8$. The inset shows the variation of the similar I^N vs N for an all-to-all model. Both show power law behavior.

both impurity-outer and outer-outer pairs showing their equivalance. Though the difference can be seen in the state $J^z = J$ where the mutual information between two outer spins vanishes in the large K limit faster than the mutual information between the impurity and any one outer spin.

3. Multipartite information

Similar to the mutual information one can calculate any higher order multipartite information to find the nature of the correlations present in different ground states. We define the tripartite information among three subsystems A, B, C as $I^3_{ABC} = (S_A + S_B + S_C) - (S_{AB} + S_{BC} + S_{CA}) + S_{ABC}$. This tripartite information scaling with the number of channels K also shown behavior similar to the mutual information case, the highest tripartite information is associated with the J^z_{min} state and saturating in the limit of $K \gg 1$. One can measure $N-$partite information for a collection of subsystems (CSS) $\{\mathcal{A}_N\} \equiv \{A_1, A_2, \cdots, A_N\}$. To define the $N-$partite information, we first define the power set of the CSS $\{\mathcal{A}_N\}$ as $\mathcal{P}(\{\mathcal{A}_N\})$, and the collection of all subsets of $\mathcal{P}(\{\mathcal{A}_N\})$ with m subsystems in it as $\mathcal{B}_m(\{\mathcal{A}_N\}) \equiv \{Q \mid Q \subset \mathcal{P}(\{\mathcal{A}_N\}), |Q| = m\}$. We also define the union and intersection of all the subsystems present in Q as $V_\cup(Q) \equiv \bigcup_{A\in Q} A$ and $V_\cap(Q) \equiv \bigcap_{A\in Q} A$ respectively. Finally, the von Neumann entanglement entropy of the subsystem A is given by S_A. Then the $N-$partite information that we are interested in is defined as

$$I^N_{\{\mathcal{A}_N\}} = \left[\sum_{m=1}^{N} (-1)^{m-1} \sum_{Q\in\mathcal{B}_m(\{\mathcal{A}\})} S_{V_\cup(Q)}\right] - S_{V_\cap(\mathcal{A}_N)} \tag{55}$$

Studying these multipartite information one can under-

stand the nature of the multiparty correlations present among the outer spins. Our study of this multi-partite information presented in the above Fig.(10) shows that the higher order multi partite information (I^N) decreases as you increase the order (N) following a power law. In the inset of the Fig.10 we have shown the similar I^N vs N behavior observed in the ground state of the all-to-all effective Hamiltonian (Eq.35). This similar power law behavior shows that one can capture the similar entanglement properties either from the stargraph or from the corresponding all-to-all model.

B. Entanglement properties of the multichannel Kondo fixed point

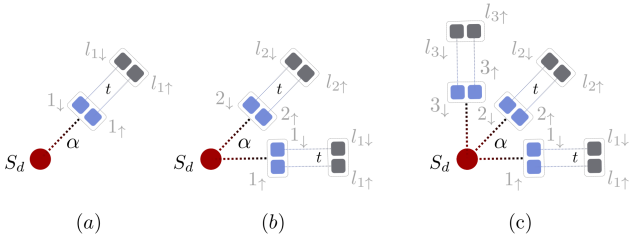

FIG. 11. This is a schematic diagram of (a) single channel and (b) two channel problem. S_d is the impurity spin. For more details refer to the text.

Apart from the entanglement study of the stargraph model, here we are interested in the entanglement entropy of the multi-channel Kondo by introducing excitations in the stargraph model. We start with the Hamiltonian Eq.(38) where we are only taking the nearest neighbor real space hopping (t) where $t = 0$ case is the zero mode Hamiltonian of the multichannel Kondo as shown in the Fig.11. In the single channel case the impurity (S_d) is talking to the spin degree of freedom at the real space origin ($\{1_\uparrow, 1_\downarrow\}$) of the unique conduction bath via a Heisenberg coupling. For 2 channel case the impurity is talking to 2 different origins of different conduction channels ($\{1_\uparrow, 1_\downarrow\}$ and $\{2_\uparrow, 2_\downarrow\}$) and hopping connects to their nearest neighbor sites, for example $\{1_\uparrow, 1_\downarrow\}$ connects to $\{l_{1\uparrow}, l_{1\downarrow}\}$. Thus, for K channel case we are solving a problem with one spin 1/2 degree of freedom and $2K$ electronic sites. As we increase the hopping strength t from zero to non-zero, the sites of the zero mode Hamiltonian starts to scatter with their respective nearest neighbor sites.

1. *Impurity entanglement entropy*

First, we are interested in the impurity entanglement entropy $EE_d(t)$ as a function of t in the ground state, shown in the Fig.12 for all the three channel cases. At low hopping strength ($0 < t \ll 1$) the EE_d is independent of t

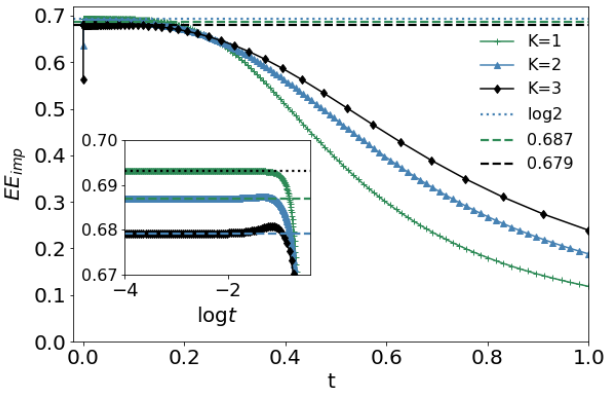

FIG. 12. This Figures shown the variation of impurity entanglement entropy EE_{imp} with the variation of the hopping strangth t for three different channel cases, $K = 1, 2, 3$.

takes a constant value, higher the channel number lower this value. On the other hand this order of EE_d changes at high t strength, where higher the channel number higher the impurity entanglement entropy. Though the impurity entanglement entropy at low hopping strength is very close to each other for different channels, the single channel impurity entanglement entropy varies smoothly with the increase of t from zero to nonzero value without any discontinuity. On the other hand for higher channels like $K = 2$ and $K = 3$ there is a discontinuity in the impurity entanglement entropy at $t = 0^+$.

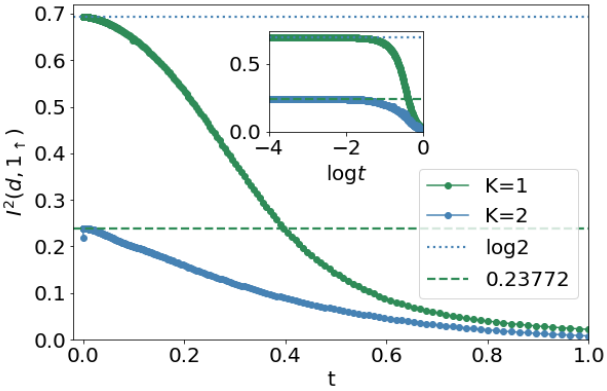

FIG. 13. This figure show the variation of mutual information between the impurity spin and $1_\uparrow$ state with respect to the variation of the hopping strength t. For more details please refer to the text. The errorbar σ_2 of the two channel data at low hopping strength $\sigma_2 \approx 0.002$.

2. *Intra-channel Mutual information*

Here we are interested in calculating Mutual information between two Fock states in the ground state wavefunction as a function of the hopping strength t varying from 0 to non zero values.

Case 1: First, we study the mutual information between the impurity spin S_d and $1_\uparrow$ Fock state (Fig.11) represented as $MI(d, 1\uparrow)$, where 1 is realspace origin of the 1^{st} conduction channel. For single channel case this $1_\uparrow$ site can be chosen uniquely but for K channel cases there are K possible choices, due to the symmetry any one choice will show similar mutual information signature. Similarly due to the $SU(2)$ spin rotation symmetry the mutual information between the impurity spin and $1_\downarrow$ state will not be any different. We have numerically computed the variation of mutual information with respect to the hopping strength t and presented in the Fig.13. As shown in the inset of the Fig.13 at low hopping strength the mutual information for both the single channel and twochannel cases is saturating at different values. In the single channel case the Mutual information for $t = 0$ is $MI(d, 1_\uparrow) = \log 2$ and changes smoothly to nozero t values, similar to the previous impurity entanglement entropy study (EE_{imp}).

$$S_d = S_{1_\uparrow} = S_{d,1_\uparrow} = \log 2\ ,\ MI(d, 1_\uparrow) = \log 2 \quad (56)$$

This $\log 2$ value shows the stability of the zero mode of single channel and perfect screening. Next we focus to the two channel case where the mutual information is $MI(d, 1_\uparrow) = 0.2401$ which is less than the single channel case showing the breakdown of screening. Note, unlike the single channel case there is a discontinuity in $MI(d, 1_\uparrow)$ at $t = 0^+$.

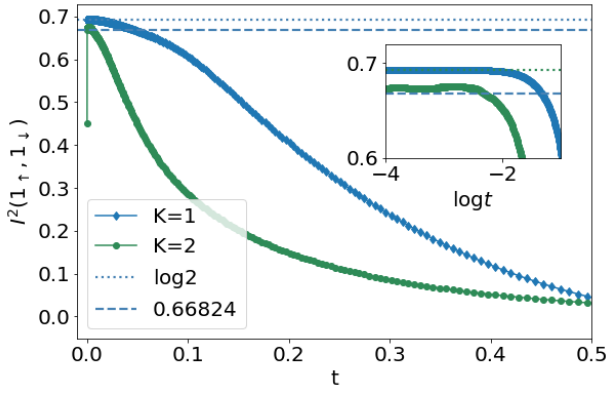

FIG. 14. This figure shows the variation of mutual information ($i^2(1_\uparrow, 1_\downarrow)$) among the two fock states present on the realspace origin (1) of a conduction channel with the hopping strength t. The errorbar σ_2 for the two channel at low hopping strength is $\sigma_2 \approx 0.013$.

Case 2: Similarly we have computed the mutual information $MI(1_\uparrow, 1_\downarrow)$ (Fig.14) which measures intra channel mutual information beteen two fock states $1_\uparrow, 1_\downarrow$ present at realspace origin. We find that the Mutual information is a smooth function of t for single channel and for two channel there is a discontinuity at $t = 0^+$. Note, $MI(1_\uparrow, 1_\downarrow) > MI(d, 1_\uparrow)$ for all t values show the presence of stronger intra-site correlation.

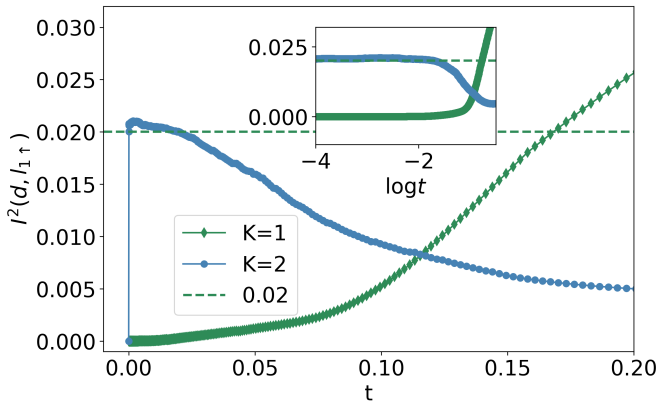

FIG. 15. Variation of the mutual information $MI(d, l_{1\uparrow})$ between the impurity spin and the $l_{1\uparrow}$ Fock state as a function of hopping strength t. The errorbar σ_2 for the two channel case is $\sigma_2 \approx 0.001$.

Case 3: Here we measure mutual information between the impurity and the Fock state of the nearest neighbor site to the realspace origin (Fig.11) of the conduction channel, $MI(d, l_{1\uparrow})$ as shown in the Fig.15. Vanishing mutual information for the single channel case shows the perfect screening of the impurity spin. On the other had we expect the breakdown of screening in two channel case, which is confirmed by the non-zero value of mutual information at small t values. Here also we find a dicontinuity inthe mutual information at $t = 0^+$.

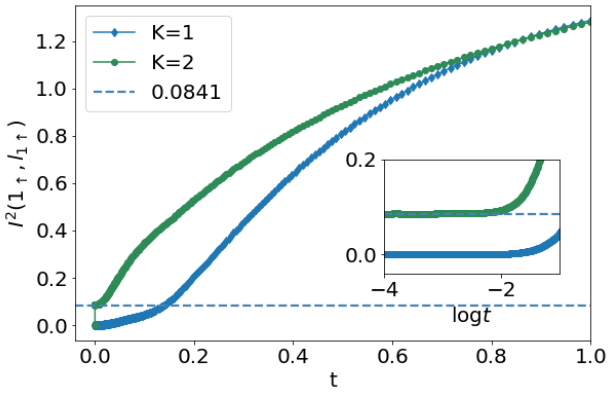

FIG. 16. Variation of the mutual information $MI(1_\sigma, l_{1\sigma})$ between two nearest neighbor sites as function of the hopping strength. The errorbar for the two channel case is $\sigma_2 \approx 0.005$.

Case 4: Another complementary study can be made by measuring the mutual information between conduc-

tion channel realspace origin and it's nearest neighbor site to check their mutual entanglement. As shown in the Fig.16, we find that at low hopping strength the single channel mutual information vanishes showing the decoupling of those two states. On the other hand in the two channel case there is a nonzero mutual information which verifies the presence of active scattering between the local Mott liquid and the local non-Fermi liquid phases. Similar discontinuity in the mutual information was observed at $t = 0^+$. Apart form the above mutual information

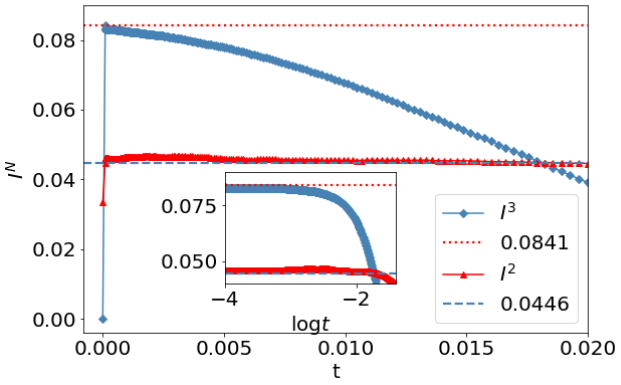

FIG. 17. Red: This is the Mutual information $I^2(1_\uparrow, 2_\uparrow)$ and the Blue is the tripartite infrmation $I^3(1_\uparrow, l_{1\uparrow}, l_{1\downarrow})$. The errorbar ($\sigma$) for the I^3 and I^2 near the low hopping strength are 0.002 and 0.003 respectively.

studies we have computed the intra-channel tripartite information $I^3(1_\uparrow, l_{1\uparrow}, l_{1\downarrow})$ of the two-channel ground state which measuring the correlation present among those three Fock states (Fig.17(blue)) which show that there is a discontinuity in the triparite information at $t = 0^+$ and at low hopping strength the tripartite information is independent of t with a value 0.084. This non-zero value of tripartie information supports the presence of non-Fermi liquid with more than two-particle correlation within. We have also studied inter-channel mutual informaition $I^2(1_\uparrow, 2_\uparrow)$ for this two channel case as shown in the (Fig.17(red)). This suggest the presence of correlation and quantum entanglement between these two channels supporting the presence of all-to-all local mott liquid.

3. *Bures distance and orthogonality catathrope*

Apart from different entanglement measures we have measured the Bures distance, which is a measure of distance between two density matrices. Which is defined as

$$d_{Bures}(\rho_1, \rho_2) = \sqrt{2}\left[1 - \mathrm{Tr}\left\{\left(\rho_1^{1/2}\rho_2\rho_1^{1/2}\right)^{1/2}\right\}\right] \quad (57)$$

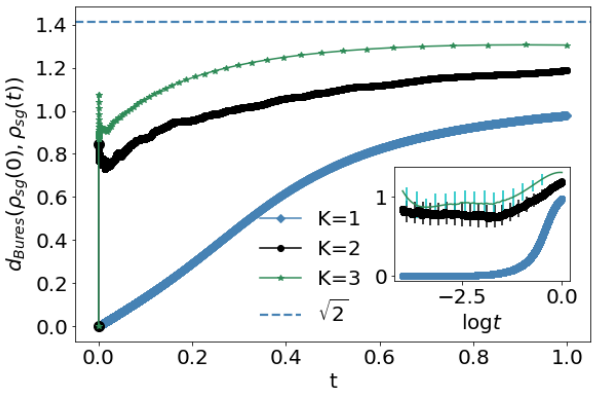

FIG. 18. Variation of Bures distance between the reduced denisty matrix of stargraph at $t = 0$ and $t \neq 0$ with the variation of hopping strength t. The errorbar (σ) of the two channel and three channel data are 0.14 and 0.08 respectively, and near $t \approx 1$ the σ is 0.04 and 0.07 respectively.

One can see from the above defination that, the maximum and minimum distance it can have is $\sqrt{2}$ and 0 respectively. This measure represents the distance between two states in a Hilbert space.

We get the ground state wavefunction of the problem by solving the Hamiltonian Eq.(38) $|\psi(t)\rangle$ which is a function of t and $\rho(t) = |\psi(t)\rangle\langle\psi(t)|$. We are interested in the reduced density matrix of the star graph sites, to get that we partial trace out all other nearest neighbor sites, $\rho_{sg}(t) = \mathrm{Tr}_{NN}(\rho(t))$. Then the Bures distance between the reduced denisty matrices $\rho_{sg}(t = 0)$ and $\rho_{sg}(t)$, denoted as $d_{Bures}(\rho_{sg}(t = 0), \rho_{sg}(t))$ are computed for single, two and three channel cases.

We have shown the variation of the Bures distance as a function of the hopping strength in the Fig.18 above. For all three cases the Bures distance is zero at $t = 0$, whic is obvious. But as you turn on t slightly there is a discontinuity in the distance for two and theree channel cases against the single channel where the distance varies smoothly. This discontinuity in the higher channel case against the single channel is similar to all the above entanglement studies. The smooth variation of the distance in the single channel case shows the adiabatic continuation of the reduced stargarph density matrix from the $t = 0$ case to $t \neq 0$ case. On the other had the abrupt jump in the Bures distance for higher-channel cases at $t = 0^+$ shows the breakdown of adiabatic continuity siganling an orthogonality catastrophe. Three channel case show higher amoount of discontinuity than the two channel case saturating at higher value for $t = 1$. Due to finite size system we cannot see the exact orthogonality by getting the $d_{Bures} = \sqrt{2}$, but higher channel cases with higher discontinuity suggests so.

All the above entanglement studies suggest that for two channel problem there is a discontinuity in the ground state at $t = 0^+$, whereas for the single channel case it is

a smooth function. Thus for single channel case the $t = 0$ and $t \neq 0$ cases can be adiabtically connected, which is not the case for any other channel cases.

VI. DUALITIES OF THE MULTICHANNEL KONDO MODEL

We start from a strong coupling ($J \to \infty$) spin-S impurity MCK Hamiltonian in the over-screened regime ($K > 2S$),

$$H(J) = \sum_{k,\sigma,l} \epsilon_{k,l} \hat{n}_{k\sigma,l} + J \vec{S}_d \cdot \vec{S} \ . \tag{58}$$

Here, $\vec{S}$ is the total spin $\sum_l \sum_{kk'\alpha\beta} \vec{\sigma}_{\alpha\beta} c^\dagger_{k\alpha,l} c_{k'\beta,l}$ of all the zero modes. At strong coupling, the ground states of the star graph eq. 8 act as a good starting point for a perturbative expansion. As argued previously, there are $K - 2S + 1$ ground states, labeled by the K values **of the total spin angular momentum** $S^z = S^z_d + S^z = -\frac{K}{2} + S, -\frac{K}{2} + S + 1, \ldots, \frac{K}{2} - S$**. To leverage the large coupling**, one can define a new spin impurity $\mathbb{S}$ out of this ground state manifold. Since the degeneracy of a spin is given by its multiplicity $2S' + 1$, we have $2S'+1 = K-2S+1 \implies S' = \frac{K}{2} - S$. That is, the spin-$S$ impurity has a dual described by a spin-$(K - 2S + 1)$ impurity. The states of this new spin are defined by

$$\begin{aligned} \mathbb{S}^z_d \left|S^z\right\rangle &= S^z \left|S^z\right\rangle, \\ \mathbb{S}^\pm_d \left|S^z\right\rangle &= \sqrt{S'\left(S'+1\right) - S^z\left(S^z \pm 1\right)} \left|S^z \pm 1\right\rangle \end{aligned} \tag{59}$$

The excited states of the star graph can be used to define bosons[32], and the hopping into the lattice can then be re-written using these Bosons. One can then remove the single-particle hoping between the zero modes and the first sites using a Schrieffer-Wolff transformation in the small coupling $J' = \gamma \frac{4t^2}{J}$, and generate an exchange-coupling between the new impurity $\vec{\mathbb{S}}_d$ and the new zero modes formed out of the remaining sites in the lattice[32] (by remaining, we mean those real space sites that have not been consumed into forming the new spin). The new Hamiltonian, characterized by the small super-exchange coupling J', has the form

$$H'(J') = \sum_{k,\sigma,l} \epsilon_{k,l} \hat{n}_{k\sigma,l} + J' \vec{\mathbb{S}}_d \cdot \vec{S'} \tag{60}$$

The prime on S indicates that it is formed by the new zero modes. This Hamiltonian is very similar to the one in eq. 58, and that is the essence of the strong-weak duality: One can go from the over-screened strong coupling spin-S MCK model to another over-screened weak coupling spin-$(K - 2S + 1)$ MCK model. For the case of $K = 4S$, we have $S' = S$, and both S_d and $\mathbb{S}_d$ describe the same spin objects (at least formally). The two models are then said to be self-dual. For example, for the case of spin-half MCK model, two-channel model is self-dual.

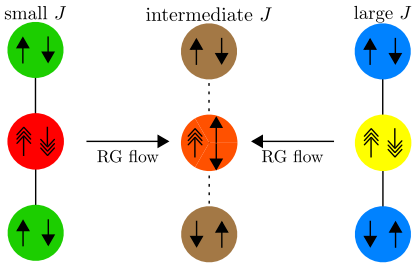

FIG. 19. Duality of the RG flows as seen in the star graph Hamiltonian. The red and green circles represent the impurity and zeroth site spins respectively. At large J, the red circle binds with the green circles to form an effective spin $\frac{K-1}{2}$ object (yellow) that interacts with the remaining spin of the conduction bath (blue circles).

One important consequence of the duality relationship between the two over-screened models is that the RG equations are also dual; while the strong coupling model has an irrelevant coupling J that flows down to the intermediate fixed point $\mathcal{J}^*$, the weak coupling model has a relevant coupling J' that flows up to the same fixed point $J'^* = \mathcal{J}^*$. From the RG equation for the general spin-S MCK model, we know that $J'^* = \frac{2}{K\rho'}$, where ρ' is the DOS for the bath of the weak coupling Hamiltonian. This constrains the form of the scaling factor γ:

$$J'^* = \frac{\gamma 4t^2}{\mathcal{J}^*} = \frac{2}{K\rho'} \implies \gamma = \frac{1}{4t^2}\mathcal{J}^{*2} = \frac{1}{K^2 t^2 \rho\rho'} \tag{61}$$

There exists another set of dual points in the MCK model. This was hinted at when we looked at the degree of compassion in eq. 12. Since Γ depends only on the magnitude of δ, both $\pm\delta$ will give the same degree of compensation, same ground state energy and same ground state degeneracy $\left(g^S_K = |\delta| + 1\right)$. The definition of δ gives the duality transformation as $K \to 2S, S \to \frac{K}{2}$. That is, we transform from a $K-$channel MCK model with spin-S impurity, to a $2S$-channel MCK with a spin-$\frac{K}{2}$ impurity. The exactly-screened model $K = 2S$ maps on to itself and is therefore self-dual under this transformation.

For $K \neq 2S$, we transform an over-screened model into an under-screened model and vice versa. This duality relationship allows us to infer the RG scaling behaviour of one of the models if we know that of the other. If we know that for a certain pair of values K and S, the $K-$channel MCK model with spin-S impurity has an intermediate fixed point, we can immediately conclude that the $2S$-channel spin-$\frac{K}{2}$ model has a strong coupling fixed point.

VII. IMPURITY QUANTUM PHASE TRANSITION IN THE MULTICHANNEL KONDO MODEL UNDER CHANNEL ANISOTROPY

RADICALLY SHORTEN AND RESTRUCTURE THIS SECTION. SHOW THE NUMER-

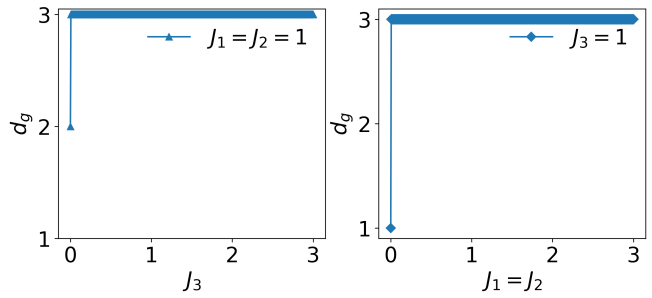

FIG. 20. *Left:* Shows the variation of the ground state degeneracy with the variation of the coupling J_3 keeping other two couplings $J_1 = J_2 = 1$ fixed. *Right:* Variation of ground state degeneracy with the variation of the couplings $J_1 = J_2$ keeping the$J_3 =$ fixed. Both these show the robustness of the ground state degeneracy against the channel anisotropy.

ICS FIRST, THEN SHOW THE RG EQUATION AND QUICKLY DISCUSS ITS CONSEQUENCES.

Here we start with a general model where the interaction strength of the impurity spin with the i^{th} outer spin is $\mathcal{J}_i$, in general $0 < \mathcal{J}_i \neq \mathcal{J}$. We start with the general coupling Hamiltonian written as

$$H_K(\vec{\mathcal{J}}) = \sum_{i=1}^{K} \mathcal{J}_i \vec{S}_d . \vec{S}_i \tag{62}$$

where $\vec{\mathcal{J}} \equiv (\mathcal{J}_1, \cdots, \mathcal{J}_K)$. For the special case $\mathcal{J}_i = \mathcal{J}, \forall i$ we get the stargraph model. For the case of spin-1/2 impurity, the Hamiltonian with any value of $\mathcal{J}_i > 0$ has K fold ground state degeneracy. This shows the robustness of the ground state degeneracy of the star graph model against the coupling anisotropy. The ground state degeneracy only changes when at least one coupling vanishes or becomes infinite. We have demonstrated this numerically for a three channel anisotropic star graph model. As shown in the Fig.20(a) where two couplings are same ($\mathcal{J}_1 = \mathcal{J}_2 = 1$) and we are varying the third coupling $\mathcal{J}_3$ from finite to zero. The degeneracy is always 3 except when $\mathcal{J}_3 = 0$, then the degeneracy becomes 2 becoming an effective two channel problem. On the other hand in Fig.20(b) we keep the first coupling $\mathcal{J}_3$ fixed to 1 and vary the common coupling $\mathcal{J}_1 = \mathcal{J}_2$ from non-zero to zero, this is equivalent to keeping $\mathcal{J}_1 = \mathcal{J}_2 = 1$ fixed and taking $\mathcal{J}_1$ to infinity from finite. In this case we find when the coupling $\mathcal{J}_1 = \lambda_2 = 0$ the degeneracy becomes one showing the effective single channel nature.

The above demonstration makes it clear that the ground state degeneracy can change only when at least one of the Kondo couplings vanish. This can be realised under RG flow if one considers the anisotropic MCK model.

$$H = \sum_{k,\alpha,l} \epsilon_{k,l} \hat{n}_{k\alpha,l} + \sum_{\substack{kk' \\ \alpha,\beta,l}} \mathcal{J}_l \vec{S}_d \cdot \frac{1}{2} \vec{\sigma}_{\alpha\beta} c^{\dagger}_{k\alpha,l} c_{k'\beta,l} \ . \tag{63}$$

We consider the specific case where $K-1$ channels have the same coupling $\mathcal{J}_1 = \mathcal{J}_2 = ... = \mathcal{J}_{K-1} = \mathcal{J}_+$ and the remaining channel has a different coupling $\mathcal{J}_K = \mathcal{J}_-$. The RG equations for such a model are

$$\frac{\Delta \mathcal{J}_\pm}{|\Delta D|} = -\frac{\mathcal{J}_\pm^2 \rho}{\mathcal{D}_\pm} + \frac{\rho^2 \mathcal{J}_\pm}{2} \left[\frac{(K-1)\mathcal{J}_+^2}{\mathcal{D}_+} + \frac{\mathcal{J}_-^2}{\mathcal{D}_-} \right] \tag{64}$$

where $\mathcal{D}_\pm = \omega - \frac{D}{2} - \frac{\mathcal{J}_\pm}{4}$ are the denominators of the URG equations. Setting $\mathcal{J}_+ = \mathcal{J}_-$ leads to the critical fixed point at $\mathcal{J}_+^* = \mathcal{J}_-^* = \mathcal{J}_* = \frac{2}{K\rho}$. We now perturb around this fixed point by defining new variables $j_\pm = \mathcal{J}_\pm - \mathcal{J}_*$. We also assume that the bandwidth is large enough so that $\mathcal{D}_\pm \simeq \omega - \frac{D}{2} - \frac{\mathcal{J}_*}{4} = -|\mathcal{D}_*|$. Performing a linear stability analysis about $j_\pm = 0$ then reveals the following two possibilities:

(a) If $j_- < 0, j_+ > 0$, the deviation j_- is relevant and $\mathcal{J}_-$ flows to zero. The flow of j_+ are constrained such that the remaining couplings $\mathcal{J}_+$ flow to the stable intermediate fixed point of the $K-1$ channel MCK model: $J_{+,*} = \frac{2}{(K-1)\rho}$.

(b) If $j_{\to} 0, j_+ < 0$, the couplings $\mathcal{J}_+$ are irrelevant, and this leads to a single channel Kondo model described by the coupling $\mathcal{J}_-$ which flows to strong coupling.

These conclusions show that the K channel intermediate fixed point is unstable under anisotropy in $\mathcal{J}_i$. If one of the couplings becomes smaller than the rest, then that coupling flows to zero while the other $K-1$ couplings flow to the $K-1$ channel fixed point. On the other hand, if $K-1$ couplings are smaller than a single coupling, then the smaller couplings vanish while the remaining coupling flows to strong-coupling.

VIII. CONCLUSIONS

[First few lines]

Using the unitary renormalization group technique we get the zero-temperature phase diagram of the multi-channel Kondo problem with an intermediate coupling fixed point. We obtain the low energy intermediate coupling fixed point Hamiltonian (LEH). At the heart of this fixed point Hamiltonian, there is a zero bandwidth problem, which is essentially a quantum mechanical stargarph problem. Many important properties of the multi-channel Kondo problem like ground state degeneracy, break down of screening can be understood by studying this zero-bandwidth stargraph problem. Impurity-field susceptibility calculations of this stargraph model show the power-law divergence at low temperatures. Thus the critical nature of the multi-channel Kondo can be understood by studying the zero-bandwidth model. Unlike the unique ground state of the single-channel problem, the presence of ground state degeneracy in the multi-channel problem allows the presence of non-local twist operators and fractional excitations in the ground state manifold. By removing the quantum fluctuations between the impurity and the rest we get to the low energy effective

Hamiltonian. The all-to-all nature of this low-energy effective Hamiltonian creates inter-channel quantum scattering in terms of electron-hole pairs creating a local Mott-liquid phase among channels. Unlike the single-channel case, this presence of local Mott-liquid is unique to the multi-channel Kondo problem.

To understand the nature of local liquid phases we add excitations on top of the zero-bandwidth stargraph model and derive the low energy effective Hamiltonian (LEH). The LEH of the 2-channel Kondo shows the absence of the Fermi liquid phase due to the exact cancellation of terms associated with two degenerate ground states. The non-Fermi liquid nature of the LEH shows the presence of strong inter-channel quantum fluctuation and the presence of the Marginal Fermi Liquid. Our study shows that ground state degeneracy is the sole reason for the presence of such non-Fermi liquid phases, which is absent in the single-channel case due to its unique ground state. Studies of various thermodynamic properties of this 2-channel Kondo LEH (presented in the supplementary material), like specific heat and susceptibility, show logarithmic dependence at low temperature which is in agreement with the literature. A similar absence of Fermi-liquid and the presence of non-Fermi liquids was observed in the three-channel Kondo problem. The above studies show the central role of ground state degeneracy in the MCK problem which makes it very different from the single-channel Kondo problem. Also, the presence of Marginal Fermi liquid shows the orthogonality catastrophe in the two-channel MCK problem, which is distinctly different from the single-channel Kondo cloud.

Various von-Neumann entanglement studies of the zero-bandwidth stargraph model show that the entanglement content is different for different degenerate ground states labeled by J^z. Impurity and outer-spin entanglement entropy with the rest at large channel limit saturate at $\log 2$ in the low J^z state opposite to the J^z_{max} state where the entanglement entropy decreases with the increase of channel number. This shows the presence of quantum fluctuations of different levels in different ground states, decreases with the increase of the J^z value. Though there was no inter-channel coupling in the multi-channel Kondo, the strong signature of inter-channel mutual information in the stargraph ground state shows the presence of inter-channel correlation in the multi-channel ground state. The power-law dependence of multi-partite information among the outer spins of the stargraph model captures the power-law behavior of the all-to-all local Mott-liquid ground state. The study of such entanglement and mutual information studies upon the addition of excitations on top of the stargraph model by tuning the real-space nearest neighbor intra-channel hopping (t) shows a discontinuity at $t = 0^+$. In contrast to the smooth behavior of various entanglement measures as a function of the hopping strength t, this discontinuity in multi-channel case signals the presence of degenerate ground state manifold and the non-Fermi liquids leading to the orthogonality catastrophe. Higher discontinuity for a higher number of channels was observed in a Bures distance study.

Intermediate coupling fixed point under the URG study along with the strong-weak duality shows the unstable nature of the couplings away from the intermediate fixed points in both the low and high coupling strength. Under the URG study, we show that in the presence of channel anisotropy some couplings become irrelevant and vanishes at the low energy fixed point. On the other hand, the study of the stargraph ground state degeneracy against channel anisotropy shows that the degeneracy only changes if one or more couplings vanishes or becomes singular. The above two studies together show that in the presence of channel anisotropy the degeneracy of the MCK does not change until the RG reaches the fixed point.

The study of the zero-bandwidth problem and systematic addition of excitation creates a template for the study of other quantum impurity systems. One can study similar multi-channel problems in the presence of interactions in the bath.

ACKNOWLEDGMENTS

The authors thank P. Majumdar, A. Mitchell, S. Sen, S. Patra, M. Mahankali and R. K. Singh for several discussions and feedback. Anirban Mukherjee thanks the CSIR, Govt. of India and IISER Kolkata for funding through a research fellowship. Abhirup Mukherjee thanks IISER Kolkata for funding through a research fellowship. AM and SL thank JNCASR, Bangalore for hospitality at the inception of this work. NSV acknowledges funding from JNCASR and a SERB grant (EMR/2017/005398).

* sp14ip022@iiserkol.ac.in
† am18ip014@iiserkol.ac.in
‡ mukherjee.anirban.anirban@gmail.com
§ slal@iiserkol.ac.in

[1] Nozières, Ph. and Blandin, A., J. Phys. France **41**, 193 (1980).
[2] A. Mukherjee and S. Lal, New Journal of Physics **22**, 063007 (2020).
[3] A. Mukherjee and S. Lal, New Journal of Physics **22**, 063008 (2020).
[4] A. Mukherjee and S. Lal, Nuclear Physics B **960**, 115170 (2020).
[5] A. Mukherjee and S. Lal, Nuclear Physics B **960**, 115163 (2020).
[6] S. Patra and S. Lal, Phys. Rev. B **104**, 144514 (2021).
[7] S. Pal, A. Mukherjee, and S. Lal, **21**, 023019 (2019).

[8] S. P. Anirban Mukherjee and S. Lal, Journal of High Energy Physics **2021** (2021), 10.1007/JHEP04(2021)148.

[9] A. Mukherjee, A. Mukherjee, N. S. Vidhyadhiraja, A. Taraphder, and S. Lal, arxiv (2021), arXiv:2111.10580 [cond-mat.str-el].

[10] J. Gan, **6**, 4547 (1994).

[11] E. Kogan, Journal of Physics Communications **2**, 085001 (2018).

[12] Y. Kuramoto, The European Physical Journal B - Condensed Matter and Complex Systems **5**, 457 (1998).

[13] A. M. Tsvelick and P. B. Wiegmann, Zeitschrift für Physik B Condensed Matter **54**, 201 (1984).

[14] N. Andrei and C. Destri, Phys. Rev. Lett. **52**, 364 (1984).

[15] G. Zaránd, T. Costi, A. Jerez, and N. Andrei, Phys. Rev. B **65**, 134416 (2002).

[16] N. Andrei and A. Jerez, Phys. Rev. Lett. **74**, 4507 (1995).

[17] A. M. Tsvelick, Journal of Physics C: Solid State Physics **18**, 159 (1985).

[18] A. M. Tsvelick and P. B. Wiegmann, Zeitschrift für Physik B Condensed Matter **54**, 201 (1984).

[19] I. Affleck and A. W. Ludwig, Nuclear Physics B **360**, 641 (1991).

[20] I. Affleck and A. W. Ludwig, Physical Review B **48**, 7297 (1993).

[21] A. W. W. Ludwig and I. Affleck, Phys. Rev. Lett. **67**, 3160 (1991).

[22] V. J. Emery and S. Kivelson, Phys. Rev. B **46**, 10812 (1992).

[23] J. von Delft, G. Zaránd, and M. Fabrizio, Phys. Rev. Lett. **81**, 196 (1998).

[24] H. B. Pang and D. L. Cox, Phys. Rev. B **44**, 9454 (1991).

[25] A. K. Mitchell, M. R. Galpin, S. Wilson-Fletcher, D. E. Logan, and R. Bulla, Phys. Rev. B **89**, 121105 (2014).

[26] V. Tripathi, Landau Fermi Liquids and Beyond (CRC Press, 2018).

[27] E. Fradkin, Field theories of condensed matter physics (Cambridge University Press, 2013).

[28] C. M. Varma and Y. Yafet, Phys. Rev. B **13**, 2950 (1976).

[29] K. Yosida, Phys. Rev. **147**, 223 (1966).

[30] K. G. Wilson, Reviews of Modern Physics **47**, 773 (1975).

[31] C. P. Moca, I. Weymann, M. A. Werner, and G. Zaránd, Phys. Rev. Lett. **127**, 186804 (2021).

[32] C. Kolf and J. Kroha, Phys. Rev. B **75**, 045129 (2007).

[33] R. Žitko and M. Fabrizio, Phys. Rev. B **95**, 085121 (2017).

[34] J. Gan, N. Andrei, and P. Coleman, Phys. Rev. Lett. **70**, 686 (1993).

[35] A. M. Tsvelick and P. B. Wiegmann, Journal of Statistical Physics **38**, 125 (1985).

[36] O. Parcollet and A. Georges, Phys. Rev. Lett. **79**, 4665 (1997).

[37] T. Kimura and S. Ozaki, Journal of the Physical Society of Japan **86**, 084703 (2017), https://doi.org/10.7566/JPSJ.86.084703.

[38] D. Bensimon, A. Jerez, and M. Lavagna, Phys. Rev. B **73**, 224445 (2006).

[39] D. L. Cox and M. Jarrell, **8**, 9825 (1996).

[40] P. Coleman, L. B. Ioffe, and A. M. Tsvelik, Phys. Rev. B **52**, 6611 (1995).

[41] P. Coleman and C. Pépin, Phys. Rev. B **68**, 220405 (2003).

[42] N. Roch, S. Florens, T. A. Costi, W. Wernsdorfer, and F. Balestro, Phys. Rev. Lett. **103**, 197202 (2009).

[43] A. Schiller and L. De Leo, Phys. Rev. B **77**, 075114 (2008).

[44] P. Durganandini, EPL (Europhysics Letters) **95**, 47003 (2011).

[45] K. G. Wilson, Rev. Mod. Phys. **47**, 773 (1975).

[46] P. Nozieres, Journal of Low Temperature Physics **17**, 31 (1974).

[47] N. Andrei, K. Furuya, and J. H. Lowenstein, Rev. Mod. Phys. **55**, 331 (1983).

[48] A. M. Tsvelick and P. B. Wiegmann, Adv. in Phys. **32**, 453 (1983).

[49] R. Bulla, T. A. Costi, and T. Pruschke, Rev. Mod. Phys. **80**, 395 (2008).

[50] A. C. Hewson, The Kondo Problem to Heavy Fermions (Cambridge University Press, 1993).

[51] C. Varma, Z. Nussinov, and W. Van Saarloos, Physics Reports **361**, 267 (2002).

[52] P. W. Anderson, Phys. Rev. Lett. **18**, 1049 (1967).

[53] K. Yamada and K. Yosida, Progress of Theoretical Physics **59**, 1061 (1978), https://academic.oup.com/ptp/article-pdf/59/4/1061/5315849/59-4-1061.pdf.

[54] K. Yamada and K. Yosida, Progress of Theoretical Physics **62**, 363 (1979).